The effects of deep cryogenic treatment on PVD-TiN coated AISI M2 high speed steel

Christian I. Chiadikobi, Rob Thornton, Dimitrios Statharas, David P. Weston

PII: S0257-8972(24)00879-X

DOI: https://doi.org/10.1016/j.surfcoat.2024.131248

Reference: SCT 131248

To appear in: *Surface & Coatings Technology*

Received date: 18 June 2024

Revised date: 12 August 2024

Accepted date: 12 August 2024

Please cite this article as: C.I. Chiadikobi, R. Thornton, D. Statharas, et al., The effects of deep cryogenic treatment on PVD-TiN coated AISI M2 high speed steel, *Surface & Coatings Technology* (2024), https://doi.org/10.1016/j.surfcoat.2024.131248

The effects of Deep cryogenic treatment on PVD-TiN coated AISI M2 high speed steel

Christian I. Chiadikobi[1], Rob Thornton[1,2]*, Dimitrios Statharas[1], David P. Weston[1]

[1] School of Engineering, University of Leicester, LE1 7RH, UK
[2] Warwick Manufacturing Group (WMG), The University of Warwick, Coventry, CV4 7AL, UK
(*rob.thornton@warwick.ac.uk)

Abstract

In this study, the effect of deep cryogenic treatment (DCT) on PVD-TiN coated AISI M2 high speed steel were investigated. DCT has been cited to improve hardness, toughness, and wear resistance in martensitic steels. Despite these promising results, there is limited published work on the effects of DCT on hard coated steels, such as industrial cutting tools. Hence, the aim of this study is dedicated to providing experimental data on the effects of PVD-TiN coated AISI M2 high speed steel subjected to DCT. A combination of microstructural and mechanical techniques, such as optical and scanning electron microscopy (SEM), transmission electron microscopy (TEM), X-ray diffraction (XRD), nanoindentation hardness and scratch testing have been applied to determine the changes observed. The result of the nanoindentation hardness showed that an improved result in terms of hardness and elastic modulus were obtained for DCT coated test samples with increases of 5.2% and 14.8% compared to conventionally prepared coated non-DCT samples. Upon further examination, it was interesting to note that there was a significant change of 14.8% in the elastic modulus of the DCT coated samples as compared with the untreated samples. The reason for the difference could be attributed to the contribution of the substrate or changes in the substrate due to DCT. For adhesion testing, optical and SEM examination revealed that DCT coated samples exhibited promising results as the transverse cracks observed for the DCT coated samples appeared denser, more extensive, and could suggest good adhesion as when the mechanical work is applied, energy is better absorbed rather than coating flaking. A comparison of the critical failure points (Lc) revealed that DCT coated samples had Lc values 3.62% high than the conventionally prepared samples, which could be attributed to the elastic modulus mismatch between the coating and substrate.

Keywords: Deep cryogenic treatment; PVD–TiN coated AISI M2 HSS; Microstructure; Elastic Modulus; Hardness; coating scratch response

1. Introduction

TiN are hard wearing coatings widely applied on industrial cutting tools (AISI M2 HSS) to improve the working life. In addition, its shiny gold appearance, provides high surface hardness, resistance to corrosion and good adhesion to cutting tools are other virtues of TiN coatings. A commonly used deposition technique for TiN coatings is through Physical vapour deposition (PVD) [1-4].

PVD coating process allows for material transfer from a solid source to the substrate, through a vacuum in vapour form, to form a coating, which is achieved at a relatively low temperature (between 50 and 450 ° C). The advantages of the coating process are numerous and also provide added benefits for its usage, such as good bond strength, uniform coating with high density structure, and good surface finish which are as good as the underlaying substrate, no issue of pollution, waste disposal, and no issue of distortion and dimensional change due to the low deposition temperature in which it carried out [2, 5].

However, to deliver additional cost savings and efficiency in the manufacturing industry, the selection of coating type, technique and substrate alone is insufficient. Strategic treatment aimed at enhancing these materials to make them last longer, stronger, tougher, or more durable is critical. In literature, one of such treatments mentioned is known as deep cryogenic treatment (DCT). DCT involves treating materials at low temperatures 193 K with the aim of causing microstructural and beneficial changes that are of great benefit in varied industries such as manufacturing, and automobile industries.

In the literature, DCT has been cited to improve hardness [6-14], fatigue life [15, 16], toughness [17-19], and wear resistance [20-23] of materials. Despite these promising results, there is limited published work on the effects of DCT on hard coated steels, such as industrial cutting tools. Much debate surrounds the topic due to the lack of consistency of results encountered and limited work being presented on mechanisms responsible for changes observed.

The aim of this study is dedicated to providing experimental data on the effects of PVD-TiN coated AISI M2 high speed steel subjected to DCT. The results obtained and reported are also discussed in other to provide input on the effects of DCT on coated AISI M2 HSS and its response compared with the conventional non-DCT coated samples.

2 Experimental Details

2.1 materials, heat treatment and preparation

AISI M2 HSS supplied by unicorn metals, UK was used as the substrate material, with chemical composition presented in Table I.

Table I: Chemical composition of AISI M2 HSS

Wt%	Mo	Cr	V	W	P	Mn	S	Si	C	Fe
AISI M2	4.86	4.2	1.89	6.05	0.33	0.33	0.01	0.31	0.89	Bal

The samples were machined to dia. 37.5 mm and thickness of 5.1mm. Heat treatment was first carried out in two steeps of preheating: first pre heating at 450 °C, then followed by second preheat at 850°C, and then continuously heated to an austenitising temperature of 1200 °C. The samples were oil quenched and tempered at 560 °C. ASTM E3-11 standard guide for preparation of metallographic specimens was followed for sample preparation. Different silica carbide papers (240 µm, 320 µm, 600 µm, 800 µm, and 1200 µm) were used to remove scratches from the surfaces. To remove the surface finish 6 µm & 1 µm was used for polishing to achieve a mirror like finish and surface roughness (Ra) of 0.04 ± 0.02 µm (obtained using sutronic 3+ surface profilometer from Taylor Hobson, UK) ready for coating deposition. The deposition of the PVD-TiN coating on the substrate were commercially performed at Teer Coatings Ltd, and then the samples to be treated were deep cryogenically treated (93 K) at Cryogenics Ltd, UK, with the company having control of the parameters used. For ease of

identification, the samples were labelled different to distinguish between them. Coated non treated samples were referred to Q+T+Coat, while treated samples were referred to as Q+T+Coat+DCT samples.

2.2 Microstructural characterisation

The morphology of the coating was studied using scanning electron microscope (SEM, FEI Quanta: FEG 650, USA), and transmission electron microscope (TEM, FEI Technai F20: FEG). The TEM samples were prepared using a focused ion beam (Helios G4 P-FIB, Thermo Fisher Scientific, USA). Elemental composition of the coating surface was determined using SEM-EDS. The coating grain size and distribution was calculated and processed using line intercept method in imageJ and OriginPRO software. X-ray diffraction was used to study the phases that were present, using Bruker D8 Advance X-ray diffractometer, with Cu Kα source, with wavelength of 0.15406 nm, scan covering initial 2θ scanning angular range from 30° to 95°, step size of 0.019478°, with 0.5 seconds count time per step. In order to estimate the induced strain and crystallite size, the Williamson-hall fitting method was used, which is achieved by examining the peak width as a function of 2θ, to deconvolute the strain and crystallite size broadening. The Williamson-hall equation is given as [24, 25]:

$$\beta_T \cos\ \theta = \ \varepsilon(4 \sin\theta) + \frac{K\lambda}{L} \quad (1)$$

Where: $\beta_T = \beta_D + \beta_\varepsilon$; and $\beta_D = \frac{k\lambda}{L \cos\theta}$; $\beta_\varepsilon = 4\varepsilon \tan\theta$; $L = \frac{k\lambda}{\beta_D \cos\theta}$

β_T: Total broadening of the peak (due to combine effect of broadening due to the crystallite size (β_D) and broadening due to strain (β_ε));

L: Average crystallite size; K: shape factor (constant 0.9) and depends on other factors such as crystal distribution and shape; β_D: full width at half maximum (FWHM) broadening of peak (radians); θ: peak positions (radians). λ: 0.15406 nm (x-ray source); ε: strain.

2.3 Mechanical characterisation

The hardness and elastic modulus were obtained using G200 nano-indenter (MTS, Nano instruments, USA, equipped with Berkovich diamond indenter tip). For this study, 36 indentation indents were conducted on each samples using a load of 50 mN to obtain the mechanical properties. The test is done by deforming the thin film on a small scale using an indenter, driven into the material, with the indenter forming an impression on the material surface. Properties are derived while continuously recording the load, displacement during one complete cycle of loading and unloading during the measurement [26-28]. Adhesion assessment of the coating surface was determined using ST200 scratch tester (Teer Coatings, Ltd, UK) fitted with a Rockwell C diamond tip. Five scratches were made on each sample, employing progressive loading testing (start load = 5 N, Maximum load = 70 N, loading rate = 100 N/min and table speed = 10 mm/min), and the average critical failure values (Lc) taken and standard deviation calculated and reported.

3 Results and Discussion

3.1 Microstructure, chemistry and morphology

The surface morphology of the coating for the non-treated (Q+T+Coat) and treated (Q+T+Coat+DCT) samples observed using SEM are shown in Figure 1. SEM micrograph of the as received AISI M2 HSS sample and resulting microstructure after hardening and tempering of the sample are shown in Appendix A.

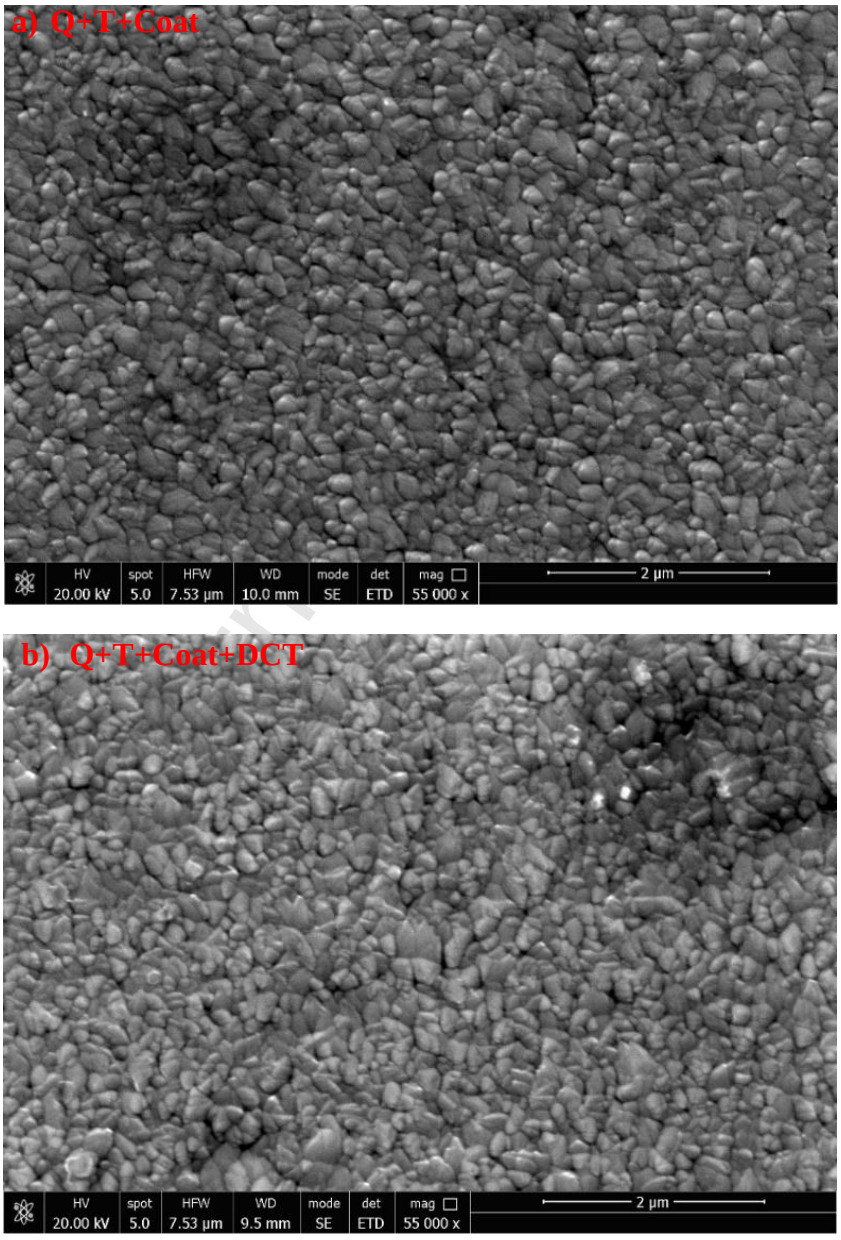

Figure 1: SEM surface morphology of the TiN coating

(a) Q+T+Coat (b) Q+T+Coat+DCT

For all cases the surface coating morphology showed a similar uniform, and dense structure typical of PVD-TiN films. The mechanism of the PVD-TiN coating is an adatom process that migrate to form clusters, which develop to form to a stable nucleus once it reaches a certain size. This then develop into a continuous uniform and dense coating structure on the substrate surface [1, 29-31].

Analysis of the grain size suggests that Q+T+Coat+DCT (161.5 ± 9.19 nm) had a slightly high grain size than Q+T+Coat (159 ± 9.19 nm) samples, however the result of the standard deviation indicated no difference between them.

For all cases, the particle size distribution illustrated in Figure 2, indicates that the data are more spread-out across the entire scale, with an occurrence rate approximately equal. On the whole, the surface roughness obtained (Table II) for the samples was found to be low and classed as smooth [32-34].

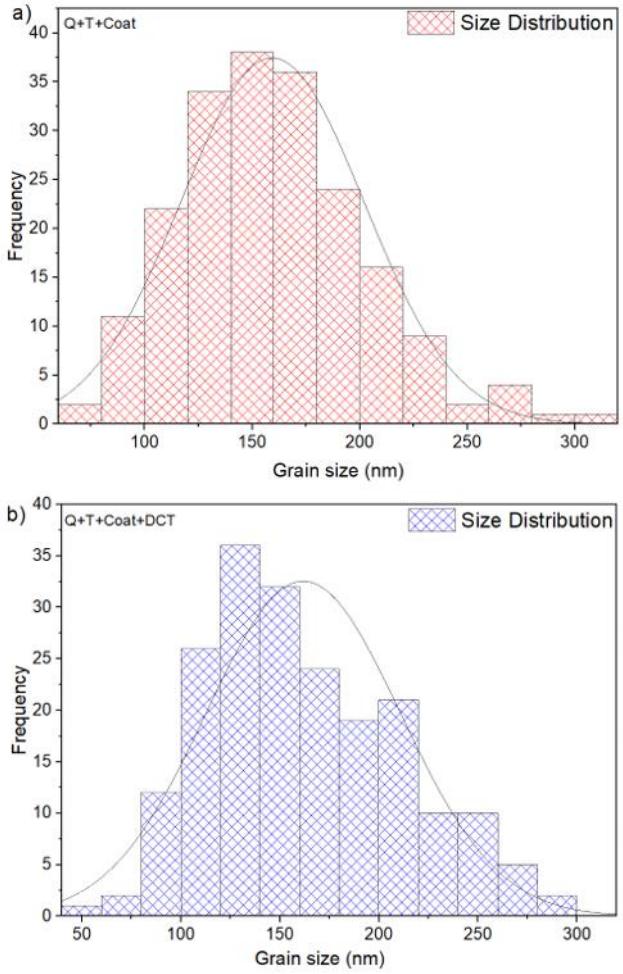

Figure 2: Coating particle size distribution

(a) Q+T+Coat (b) Q+T+Coat+DCT

Table II: Average surface roughness

Surface Roughness	**Ra Value**
Theoretical value	(0.02 – 0.09) ± 0.05 µm
Experimental value: Q+T+Coat	0.0514 ± 0.001 µm
Experimental value: Q+T+Coat+DCT	0.0519 ± 0.001 µm
Experimental value: Q+T	0.04 ± 0.002 µm

On the cross section (Figure 3), EDS line scan indicates no difference between Q+T+Coat and Q+T+Coat+DCT samples. SEM-EDS revealed that coating had a content of both Ti and N. The overall average coating thickness (Figure 4) composed of Ti (thin underlayer) and TiN

(thick layer) was 2.33 ± (0.01) µm. The Ti underlayer was added in order to promote adhesion of the coating to the substrate.

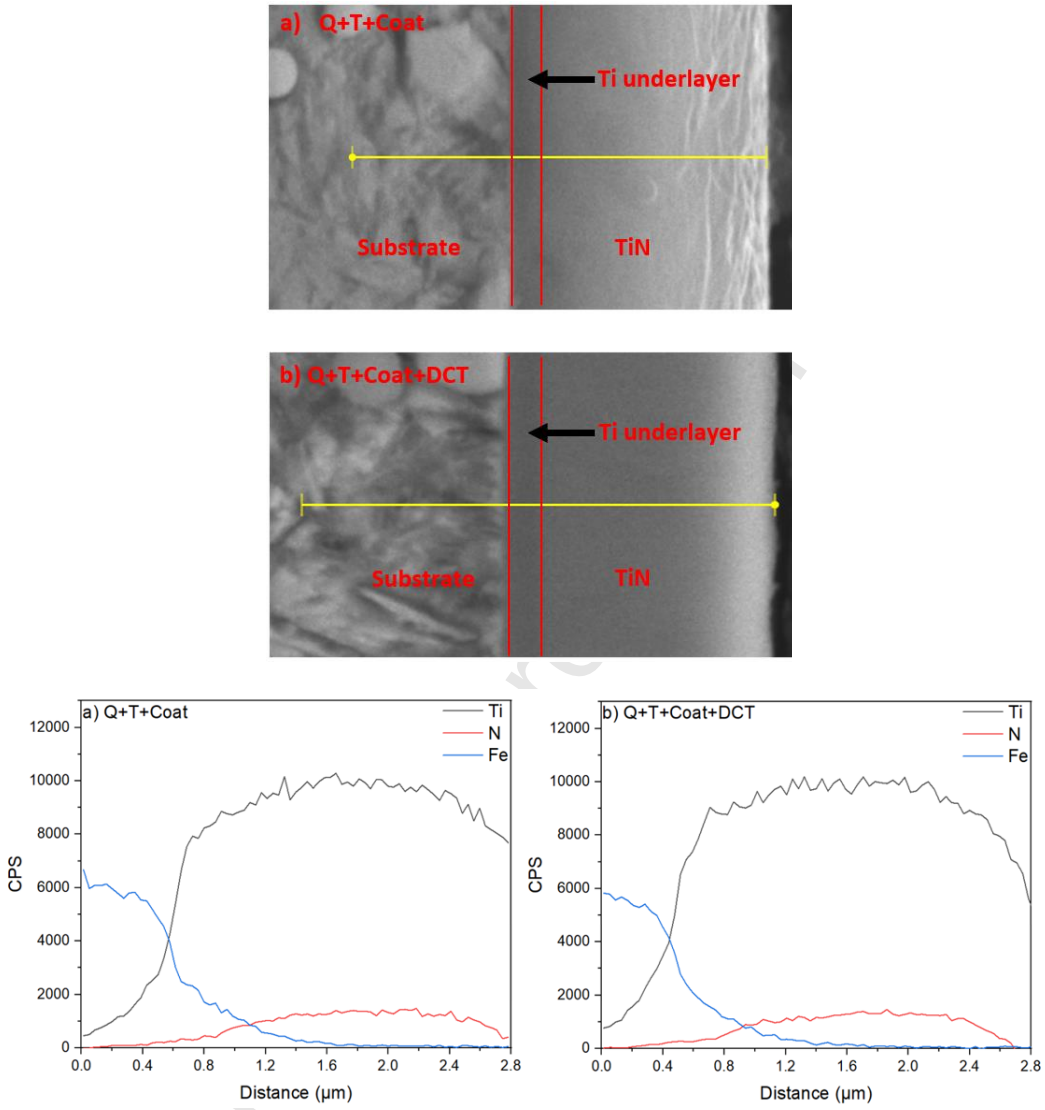

Figure 3: EDS line scan (a) Q+T+Coat (b) Q+T+Coat+DCT

For Q+T+Coat and Q+T+Coat+DCT samples, the distribution of the elements appeared to be similar. From the surface of the coating Ti, N kept a constant value along the distance suggesting to be evenly distributed. Decline of the coating was observed as the coating thickness ends, while the Fe increased into the substrate.

Regardless of the case (Q+T+Coat and Q+T+Coat+DCT samples) no difference was observed in the elemental composition (Table III).

Table III: SEM-EDS elemental composition and coating thickness

Samples	Elemental composition (wt%)	Coating thickness
Q+T+Coat	Ti: 77.24; N: 22.76	2.33 ± (0.05) µm
Q+T+Coat+DCT	Ti: 78.26; N: 21.74	2.33 ± (0.03) µm

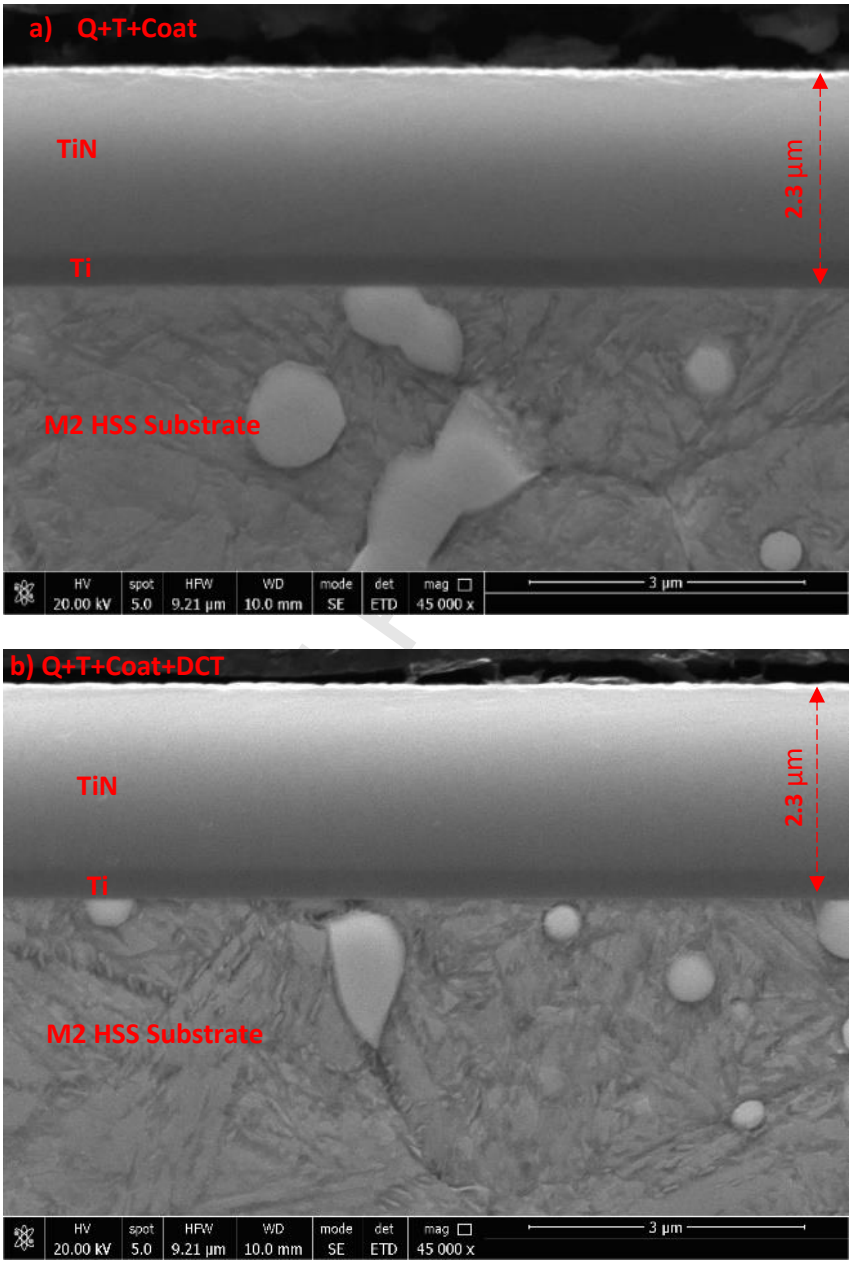

Figure 4: SEM micrograph of the coating cross-section (a) Q+T+Coat (b) Q+T+Coat+DCT

In other to obtain further information on the cross section, for both cases TEM micrograph revealed that the coating was characterised by columnar microstructure, that extends throughout the entire thickness as shown in Figure 5.

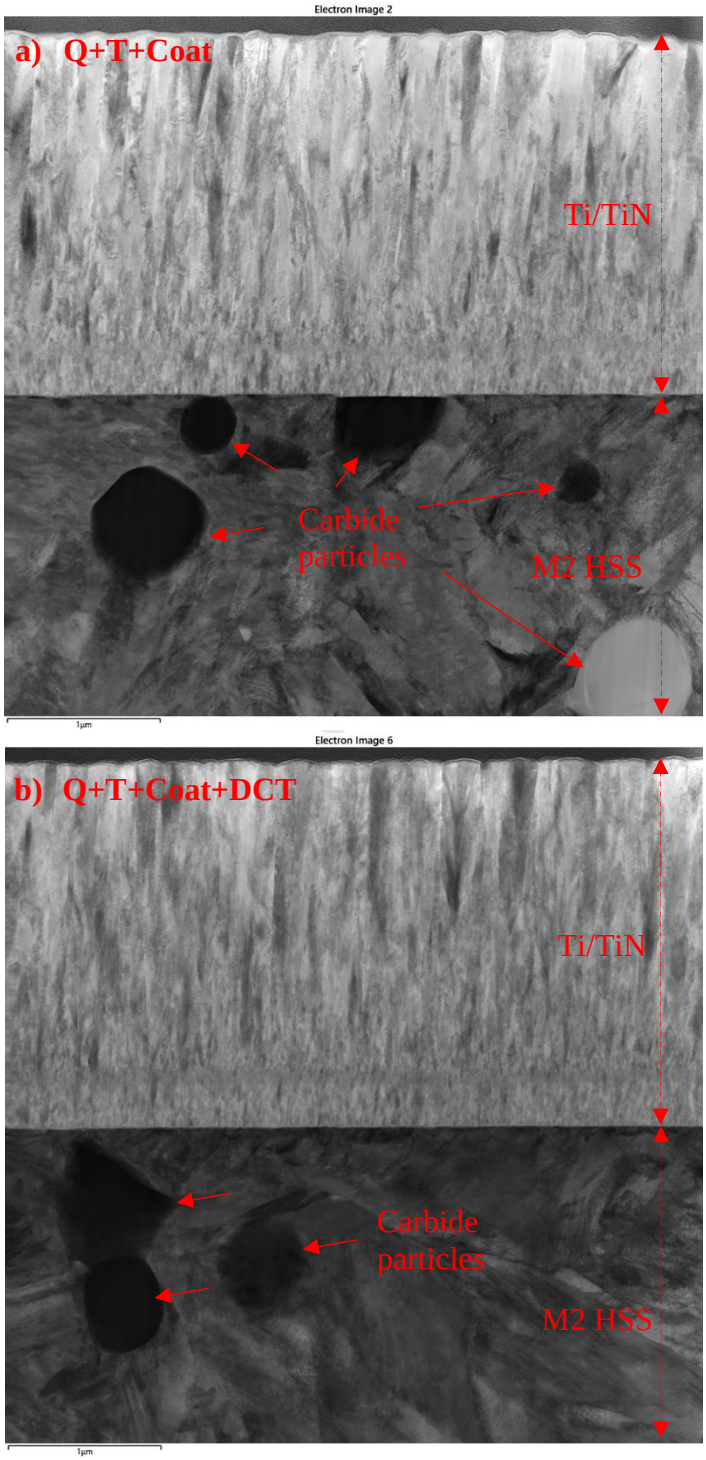

Figure 5: TEM micrograph of the coating cross – section

(a) Q+T+Coat (b) Q+T+Coat+DCT

Both structures appeared dense and compact which could be correlated which could be correlated to the SEM micrograph in Figure 1 revealing that the topography of the coating surface matched the exterior surface in term of appearance, which was dense and compact.

The x-ray diffraction spectra obtained for the samples are shown in Figure 6. The result show that both samples exhibited identical XRD patterns.

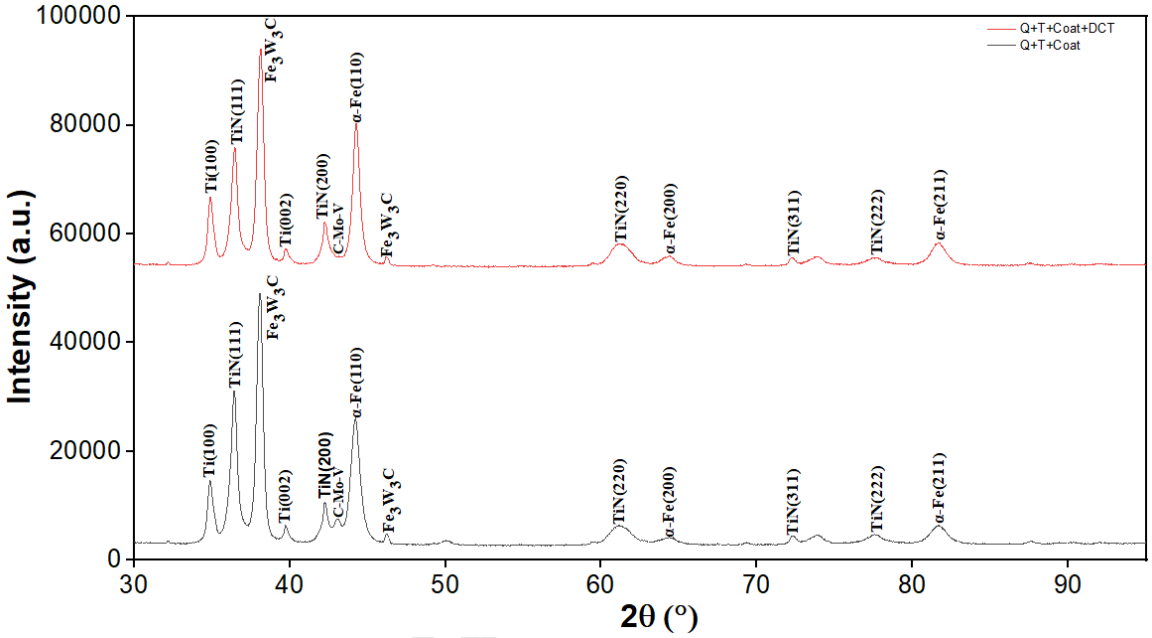

Figure 6: XRD patterns of the samples

The TiN coating showed reflections corresponding to (111), (200), (220), (311) and (222), was found at 36.51°, 42.57°, 61.37°, 72.26° and 77.56° respectively. Regardless of the case, the TiN coating exhibited a preferred orientation of (111), which is typical of TiN films deposited on AISI M2, suggesting relieving strain [35]. Diffraction peaks in the 2θ angle, at 34.85° and 38.66° that corresponds to (100) and (002) was found for Ti underlayer.

Due to the thickness of the coating, some of the diffraction pattern observed were also from the AISI M2 substrate. Reflection corresponding to (110), (200) and (211) found at 44.25°, 64.37° and 81.62° respectively was for AISI M2 substrate.

Peak at 2θ angle of 42.97° was found for C-Mo-V carbide, while in the 2θ angle of 38.14°and 46.26° was found to be Fe_3Mo_3C carbide type, with the strongest peak at 38.14°. It was unclear as to why the strongest peak was from the carbide. Given that this is part of the substrate contributions (combination of carbide), this may well be valid as the coating thickness (2.3 µm) is very thin for XRD measurement (minimum layer thickness for XRD is 7 µm), and hence incorporates information from the substrate and dwarfs the coating peaks. Therefore, it could be recommended as a future work to use glazing angle scan to see if it will limit penetration of x-rays into the sample.

In other to further understand the contributions of the substrate surface and on the growth of the coating, interplanar distances (d) and lattice parameters (a) of the substrate and coating were compared and result presented in Table IV and V.

Table IV: Interplanar spacing and lattice parameters of TiN planes

Crystalline Planes	**2θ (°)**	**Q+T+Coat: d (nm)**	**Q+T+Coat+DCT: d (nm)**	**Q+T+Coat: a (nm)**	**Q+T+Coat+DCT: a (nm)**
(111)	36.51°	0.243± 0.05	0.245±0.05	0.428±0.001	0.425±0.001
(200)	42.57°	0.212±0.05	0.213±0.05	0.425±0.001	0.425±0.001
(220)	61.37°	0.151±0.05	0.151±0.05	0.428±0.001	0.427±0.001
(311)	72.26°	0.129±0.05	0.128± 0.05	0.427±0.001	0.425±0.001
(222)	77.61°	0.123±0.05	0.123±0.05	0.426±0.001	0.426±0.001

Table V: Interplanar spacing and lattice parameters of the substrate (α-Fe) planes

Crystalline Planes	**2θ (°)**	**Q+T+Coat: d (nm)**	**Q+T+Coat+DCT: d (nm)**	**Q+T+Coat: a (nm)**	**Q+T+Coat+DCT: a (nm)**
(110)	44.25°	0.205±0.04	0.205±0.04	0.290±0.001	0.290±0.001
(200)	64.37°	0.145±0.04	0.145±0.04	0.289±0.001	0.290±0.001
(211)	81.62°	0.118±0.04	0.118±0.04	0.289±0.001	0.290±0.001

As can be seen, interplanar distances and lattice parameters of the substrate and that of the coating values are approximately equal between Q+T+Coat and Q+T+Coat+DCT samples. The similarity in results suggests that there is a little degree of mismatch between the crystal planes, which could also imply little amount of stress in the systems [35], suggesting there is no microstructural change at the interface following DCT. Following from this, important information has emerged that DCT does not appear to have an effect at the interface. A possible reason for this interpretation is that for non-DCT coated system, difference in thermal expansion coefficients could cause stresses between the system [36, 37]. Established results reported elsewhere [8, 21] suggests the substrate could undergo certain microstructural changes such as the conversion of retained austenite to martensite. This will potentially affect the interface. Nevertheless, from this investigation it was clear that no change was observed in the lattice parameter, therefore implying no effect at the interface.

By further examining the microstructure extracted from the XRD data, the result from Williamson Hall fitting plot used to estimate the strain the crystallite size is shown in Figure 7 and 8.

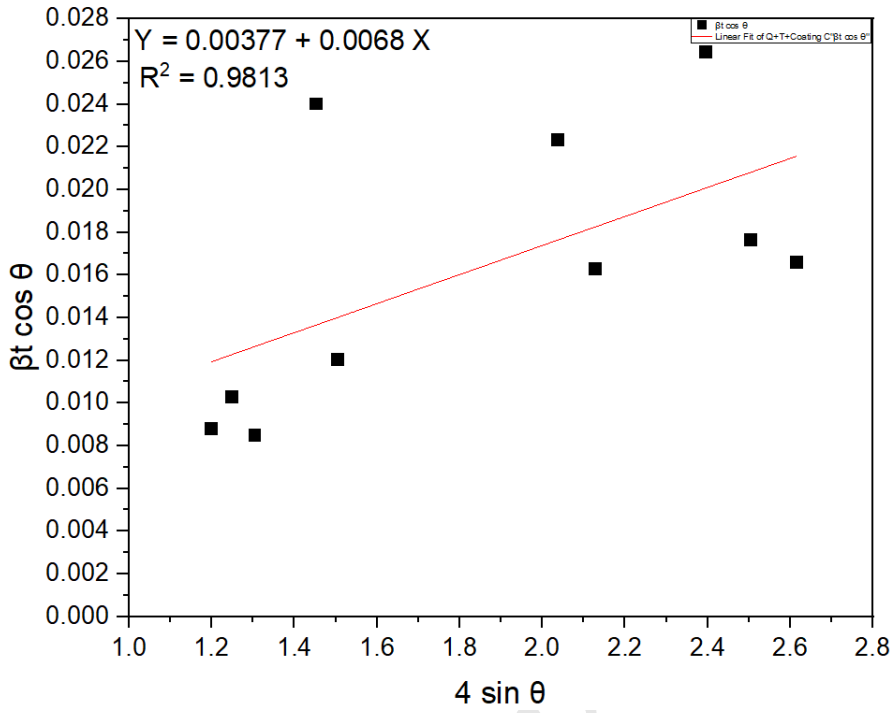

Figure 7: Plot of βt cos θ against 4 sin θ for Q+T+Coat

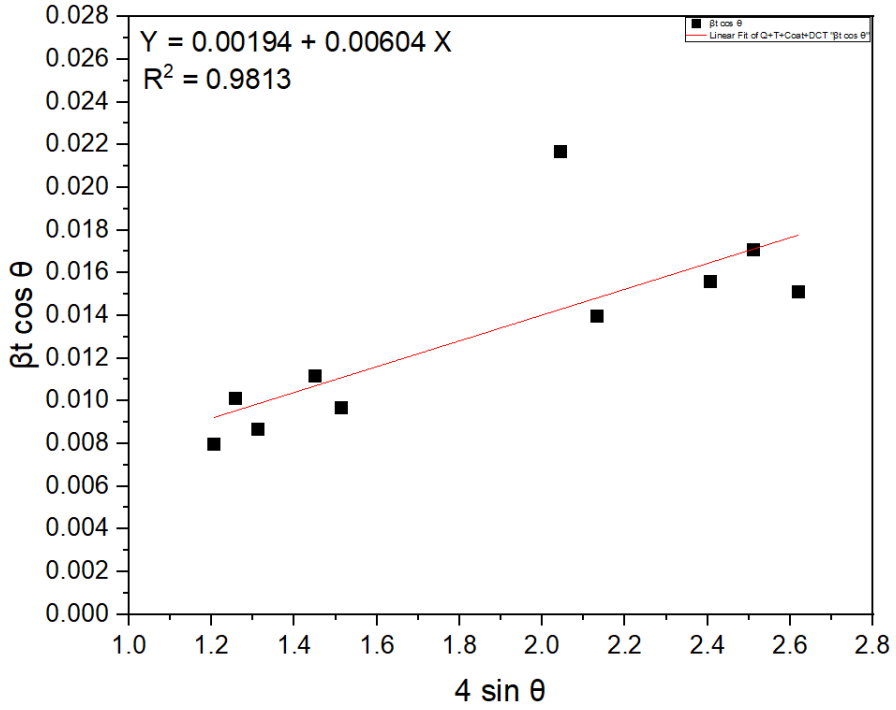

Figure 8: Plot of βt cos θ against 4 sin θ for Q+T+Coat+DCT

For Q+T+Coat, the trend in the data show more scatter and away from the linear fit as against Q+T+Coat+DCT in the x-axis, while for Q+T+Coat+DCT the data spread is over a wider area along the linear fit than in Q+T+Coat. In all examination, a comparison of the R^2 (coefficient

of determination) values to determine the correlation of the data, showed that both graphs predict an accuracy of 0.981.

The average crystallite size obtained for Q+T+Coat samples was 9.91(±4.11) nm and strain of 0.0068 (±0.00331) %, while the average crystallite size obtained for Q+T+Coat+DCT samples was 11.64 (±3.66) nm and strain of 0.00604 (±0.00175). Suggesting a slight increase in crystallite size accompanied by a decreased strain for DCT coated samples in comparison to non-DCT samples that exhibited a reduced crystallite size but increased strain. An increase in strain implies a variety of crystalline defects such as excessive grain boundaries arising due to dislocations [24, 38, 39].

3.2 Modulus and Hardness

Table VI and VII presents the mechanical properties (hardness and elastic modulus) results obtained from the nano-indentation test and t-statistics.

Table VI: Hardness and modulus of the samples

Material condition (Coating/substrate)	**Elastic Modulus (GPa)**	**Indentation Hardness (GPa)**	**Elastic Modulus ratio (GPa) Eco/Esu**
Q+T+Coat	267.46 ± 13.40	20.15 ± 1.46	--
Q+T+Coat+DCT	307.07 ± 14.05	21.19 ± 1.34	--
Q+T	169.41 ± 17.56	7.14 ± 1.21	--
Q+T+DCT	184.54 ± 13.06	7.86 ± 0.80	--
Q+T+Coat – Eco/Esu	--	--	1.58 ± 0.04
Q+T+Coat+DCT - Eco/Esu	--	--	1.66 ± 0.04

Table VII: T - statistics

T-statistics (Q+T+Coat & Q+T+Coat+DCT) Modulus **(P-value)**	**T-statistics (Q+T & Q+T+DCT) Modulus** **(P-value)**	**T-statistics (Q+T+Coat & Q+T+Coat+DCT) Hardness** **(P-value)**	**T-statistics (Q+T & Q+T+DCT) Hardness** **(P-value)**
2.2572E-19 (Significant)	4.67168E-05 (Significant)	0.001248 (Significant)	0.002026 (Significant)

The result indicates that DCT coated samples (Q+T+Coat+DCT) had a high elastic modulus (14.8%) and hardness (5.16% increase) compared to non-DCT coated (Q+T+Coat) samples. Similarly for the substrate, an increase of 8.93% and 10.04% was recorded for elastic modulus and hardness.

Upon further examination, it was interesting to note that there was a significant change of 14.8 % in the elastic modulus of the DCT coated samples as compared with the untreated samples. This result appeared to be high, and also given that the coating thickness was thin (2.33 ± 0.01) µm), as well as no clear microstructural change observed on the surface morphology (Figure 1) and cross section (Figure 3 and 4) to suggest the reason for the difference. However, it seems likely that the difference could be attributed to the contribution of the substrate or changes in the substrate due to DCT. There is lack of microstructural evidence in literature on the PVD-TiN AISI M2 HSS following DCT, to compare this result and interpretation directly as to the reason for the significant change obtained on the coating elastic modulus.

Further examination on the ratio of elastic modulus to examine the coating - substrate combination, the result indicates a minimum mismatch was observed between the systems for both DCT coated samples and non-DCT coated samples, and with the result suggesting that

DCT coated samples gave an improved elastic modulus ratio (Eco/Esu: 5.06% increase), which could suggest better resistance to wear than the non-DCT sample.

In order to further ascertain the accuracy of the data, T-statistics evidenced that the results are significant and the critical value, $P < 0.05$, implying there is a 99.9% confidence interval for Q+T+Coat and Q+T+Coat+DCT samples data, hence giving more confidence on data experimental data collected. On the substrate between Q+T and Q+T+DCT samples, the standard deviation suggests an overlap in the data, but further performing the t-statistics the data suggests there were differences as p value was observed to be low (< 0.05%), and given the number of indents (36 indents) taken per sample, the low p values obtained are well valid.

The surface morphology of the nano indentation impression for Q+T+Coat and Q+T+Coat+DCT samples as observed by SEM is shown in Figure 9.

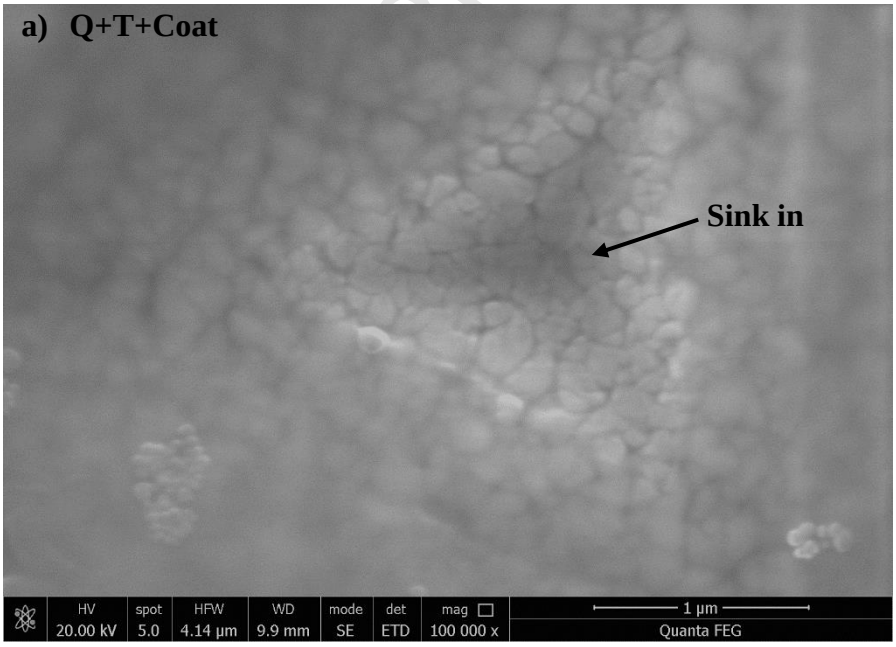

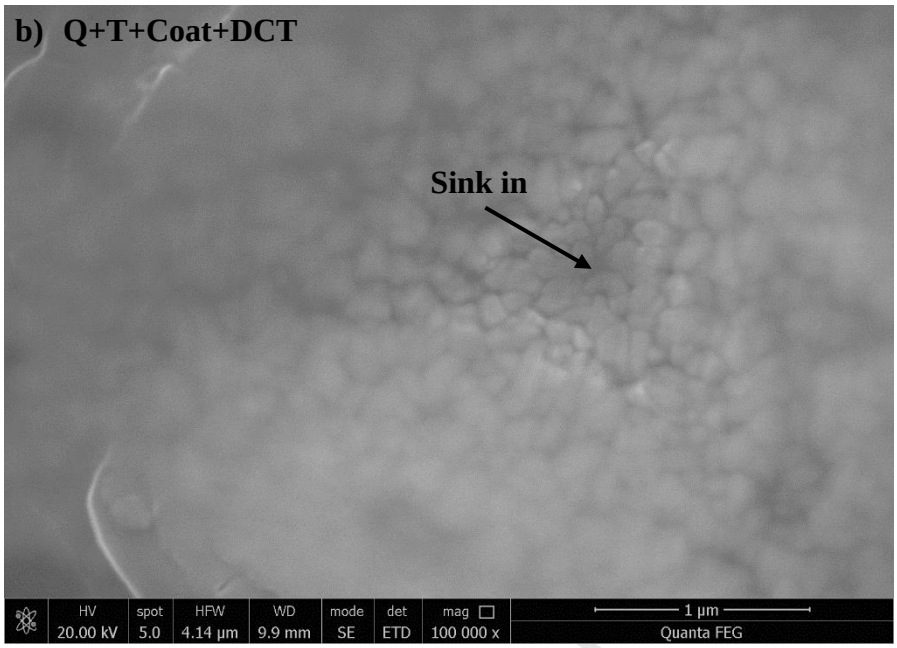

Figure 9: SEM micrograph of indentation impression made in (a) Q+T+Coat (b) Q+T+Coat+DCT sample

For both samples, the micrograph revealed slight sink-in impression and material extrusion, but less pronounced for Q+T+Coat+DCT compared with Q+T+Coat sample.

Around the edges (Figure 10), the micrographs revealed that both samples exhibited fracture induced cracks at the corners of the imprint, which could suggest brittle failure typical of TiN coatings.

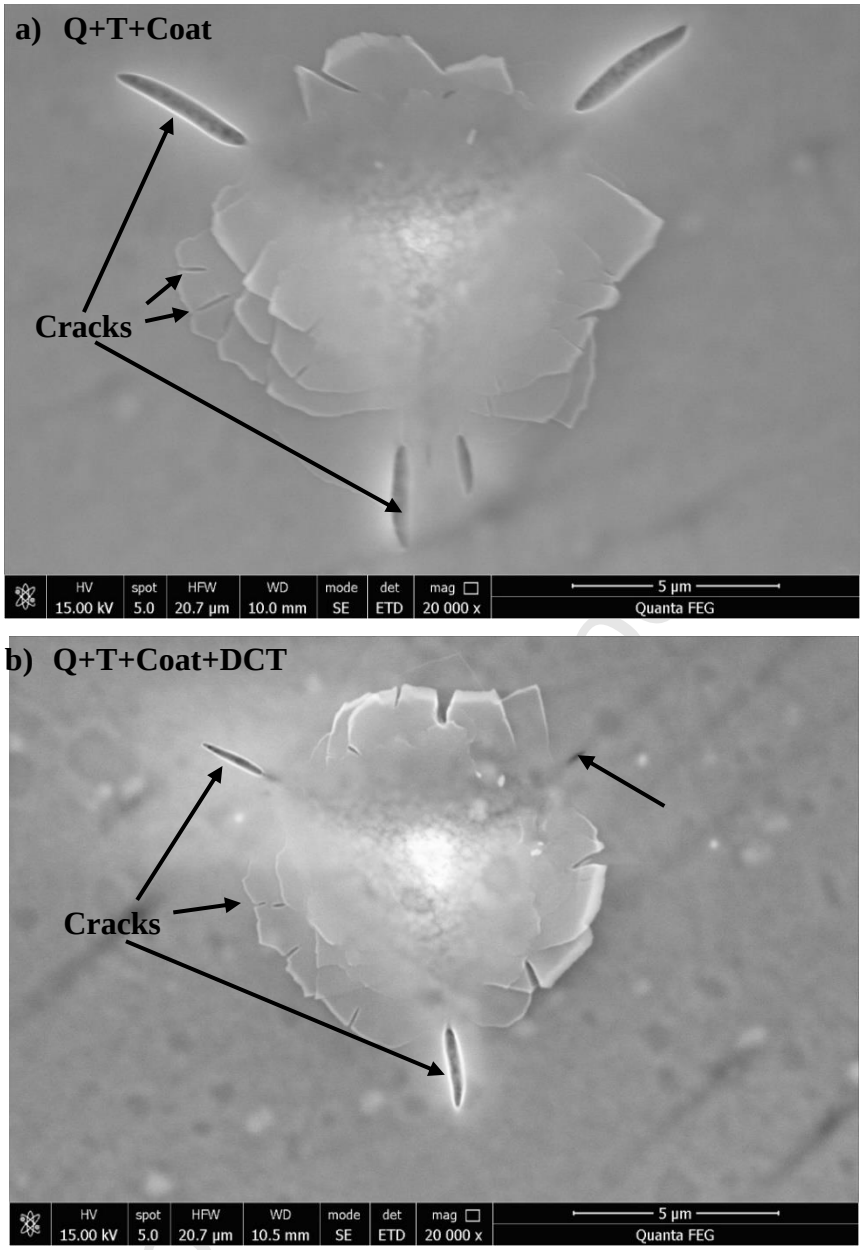

Figure 10: SEM micrograph showing cracks around the edges of the imprint
(a) Q+T+Coat (b) Q+T+Coat+DCT sample

The size of the fracture for Q+T+Coat+DCT sample was longer (3.35 ± 0.54 µm) and wider (0.50 ± 0.19 µm) than for Q+T+Coat+DCT sample that was found to be 1.85 ± 0.22 µm in length and 0.23 ± 0.07 µm in width, suggesting that the latter had better resistance to crack, thereby demonstrating the material tough nature. And therefore, supports the findings presented in Table VI and VII.

3.3 Scratch response

Figure 11 (a – d): Q+T+Coat and 12 (e – h): Q+T+Coating+DCT, presents the images of the scratch tracks of the samples. A combination of chevron, perpendicular (transverse), tensile cracks and failures (complete coating removal) were observed for all samples, and differentiated by their Lc values. In the examination, three critical failures such as Lc 1, Lc 2 and Lc 3 points were taken for the different samples as observed. Lc1 is defined as load where first recognisable failure observed, load where second failure was referred to as Lc 2, while load at which the coating was completely exposed was labelled as Lc 3. A summary of the Lc values obtained and standard deviation are presented in Table VIII.

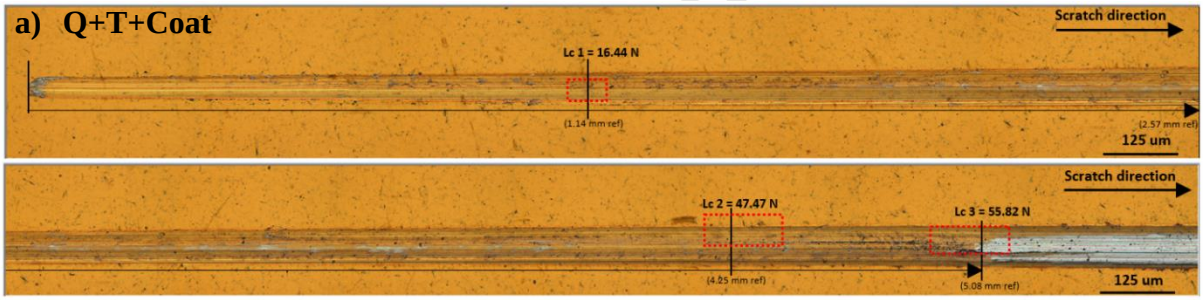

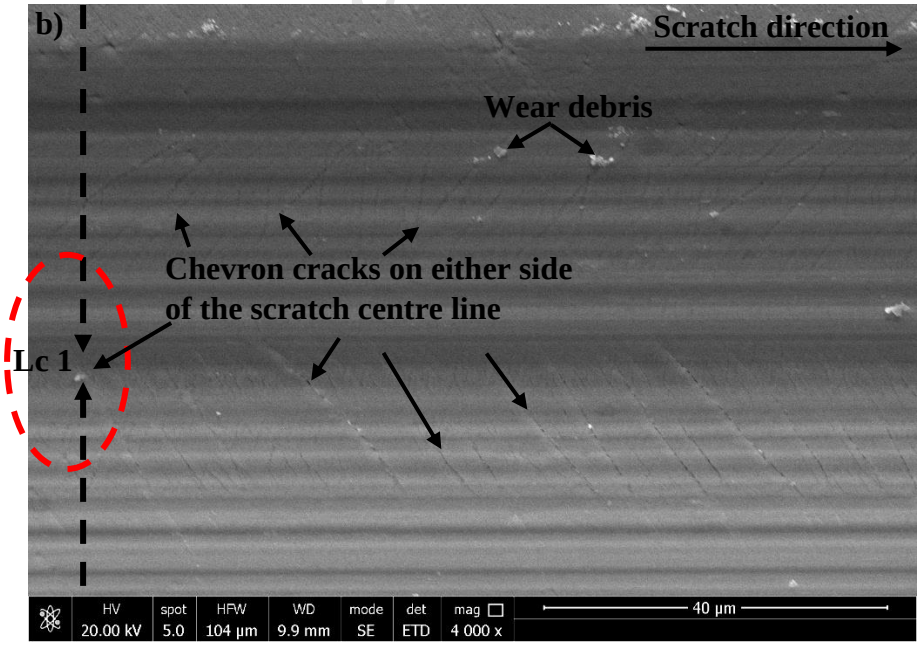

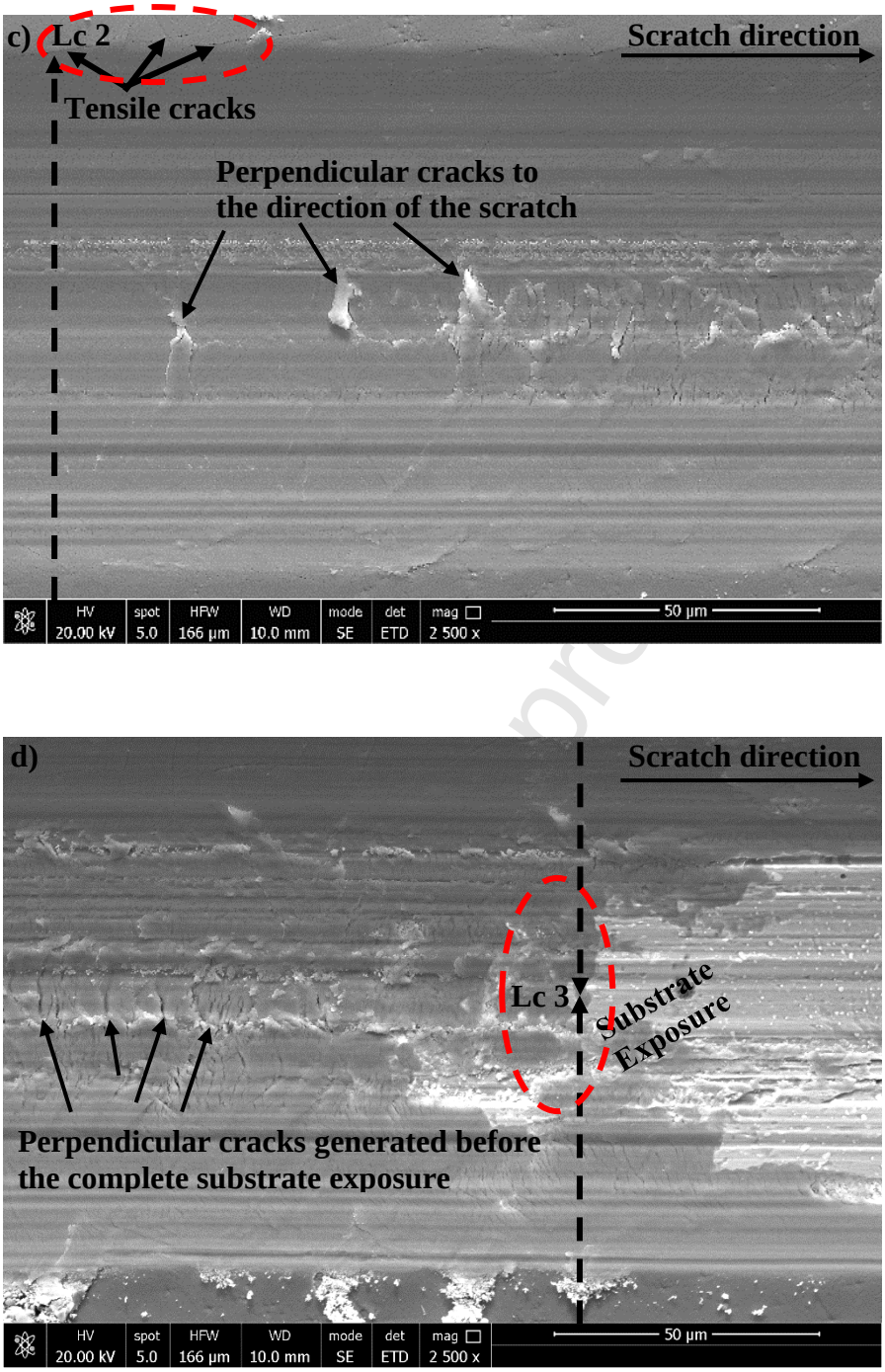

Figure 11: (a) Split-up image from optical microscope showing the scratch tracks from complete to the substrate exposure for Q+T+Coat sample. SEM micrograph showing the Lc positions and cracks observed: (b) Lc 1 – 16.44 N (c) Lc 2 – 47.47 N (d) Lc 3 – 55.82 N

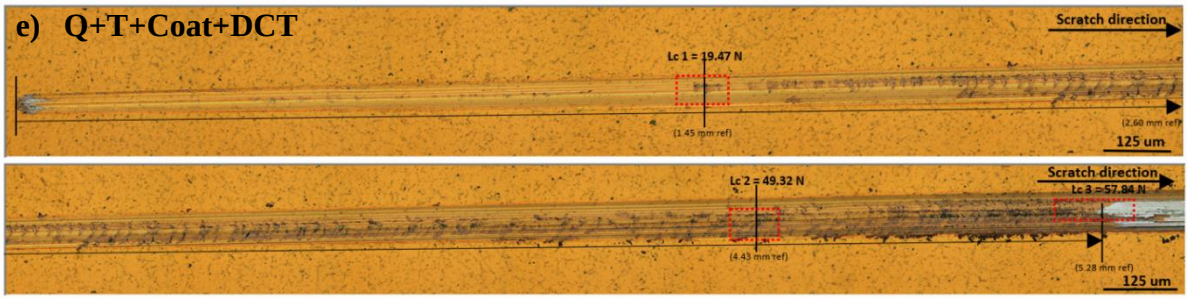
e) Q+T+Coat+DCT
Scratch direction
Lc 1 = 19.47 N
125 um
Lc 2 = 49.32 N
Scratch direction
125 um

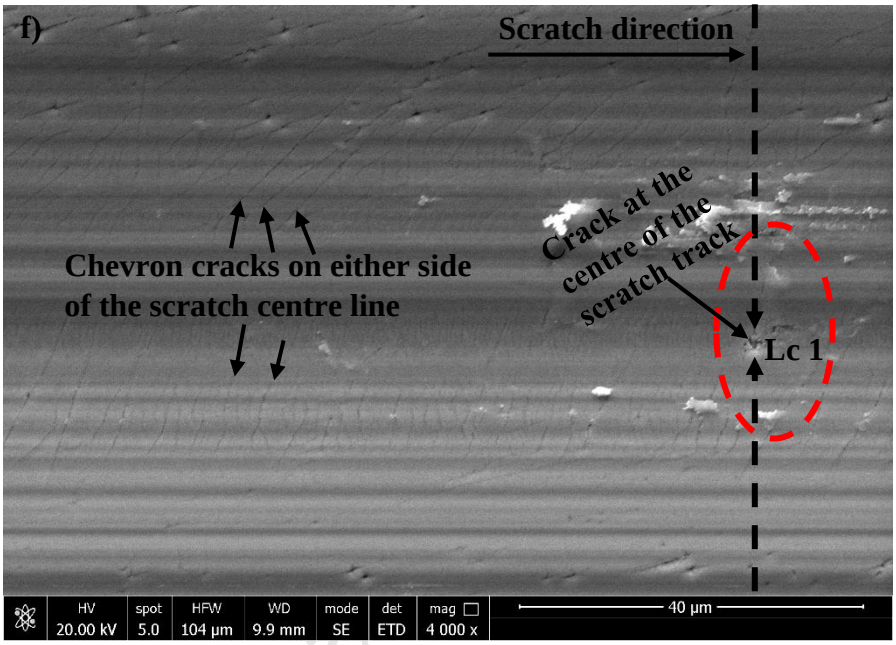
f)
Scratch direction
Chevron cracks on either side of the scratch centre line
Crack at the centre of the scratch track
Lc 1
HV 20.00 kV
spot 5.0
HFW 104 µm
WD 9.9 mm
mode SE
det ETD
mag 4 000 x
40 µm

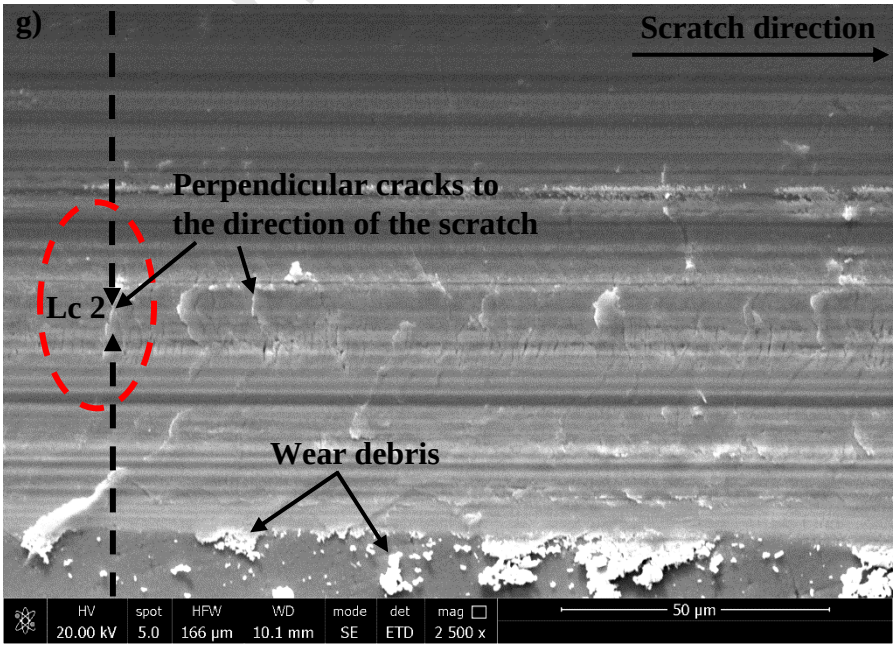
g)
Scratch direction
Perpendicular cracks to the direction of the scratch
Lc 2
Wear debris
HV 20.00 kV
spot 5.0
HFW 166 µm
WD 10.1 mm
mode SE
det ETD
mag 2 500 x
50 µm

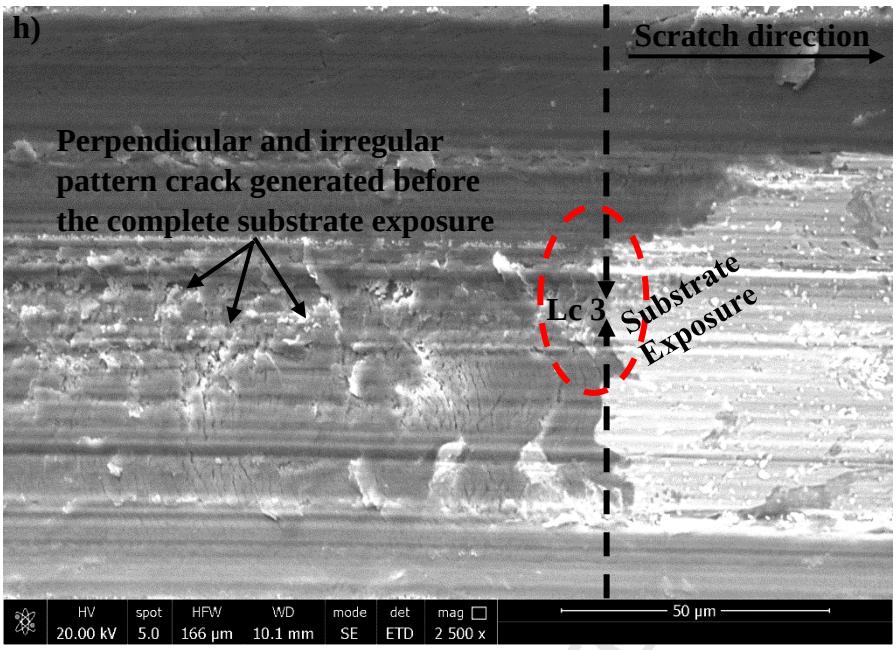

Figure 12: (e) Split-up image from optical microscope showing the scratch tracks from complete to the substrate exposure for Q+T+Coat+DCT sample. SEM micrograph showing the Lc positions and cracks observed: (f) Lc 1 – 19.47 N (g) Lc 2 – 49.32 N (h) Lc 3 – 57.84 N

Table VIII: Summary of Lc values and standard deviation

Samples	Lc 1 (N)	Lc 2 (N)	Lc 3 (N)
Q+T+Coat	16.44 ± 2.08	47.47 ± 2.03	55.82 ± 2.92
Q+T+Coat+DCT	19.47 ± 1.70	49.32 ± 2.02	57.84 ± 3.11

At Lc 1 (16.44 ± 2.08 N) – Figure 11 (a and b), mild chevron cracks were detected for the Q+T+Coat samples. These cracks from on either side of the scratch centreline, appearing to be short and long at an acute angle to the direction of the scratch. As the load reached 47.47 ± 2.03 N (Lc 2), tensile cracks were observed along the scratch edge parallel to the direction of the scratch track. As well as cracks that formed on the scratch centreline, perpendicular to the scratch track. In addition to signs of abrasive wear that progressed into Lc 3 (55.82 ± 2.92 N – complete substrate exposure).

In the Q+T+Coat+DCT samples, first critical load (Lc 1) occurred at 19.47 ± 1.70 N (Figure 12e and f). Similarly, chevron cracks that form on either side of the scratch centreline as well

as cracks that form on the centre of the scratch. For all samples (comparison between Q+T+Coat and Q+T+Coat+DCT samples), the chevron cracks that form are typical failure modes for PVD-TiN coatings and occur for ductile substrate materials and at high load [40].

As can be seen from Figure 12g, at Lc 2 (49.32 ± 2.02 N), an irregular crack pattern was observed at the centre of the track. The crack appears to fit into the track, open away and perpendicular to the direction of the scratch, and could be interpreted as internal transverse cracks. It has been suggested [41] that these cracks are often observed during scratching, as under and around any contact tensile stresses are generated behind the moving indenter tip, hence resulting in these crack type on sliding.

Further investigation as to these cracks (Lc 2) showed that for Q+T+Coat+DCT samples, the cracks appeared to be denser and extensively propagated when compared with Q+T+Coat samples. This difference in the result was attributed to the improved mechanical properties - hardness and elastic modulus of the system. As a result, has generated high tensile stresses and compressive stresses at the back of the moving indenter respectively. The combined effect of the stresses results in the perpendicular micro-cracks that form. Similar behaviour in PVD-TiN coating on Vandis Tool study [32], suggesting adhesion is good, as when the mechanical work is applied, energy is better absorbed instead of the coating flaking. The larger the region the coating adheres.

In addition, a comparison made between Q+T+Coat (Figure 11c) and Q+T+Coat+DCT (Figure 12g) suggests that despite the coating damage, the cracks that occurred for the coated treated samples appeared to be smoother than that of coated non-treated samples. For both cases (Figure 11c, d, 12g and h), short deformation ridges were observed in the direction of the scratch, that was initially restricted to a small area but later progresses to cover the entire length.

Suggesting ductile behaviour. However, the deformation ridges appeared less pronounced for DCT coated samples than its corresponding counterpart.

At Lc 3 (57.84 ± 3.11 N), complete exposure of the substrate was observed. A comparison of the critical failure points showed that Q+T+Coat+DCT samples had Lc values 3.62 (± 3.02) % higher than Q+T+Coat samples, which could be attributed to the elastic modulus mismatch between the coating and substrate, suggesting adhesion strength was better for DCT coated samples with high critical values as can be seen in Table VIII than for non-DCT coated samples. Confirming this behaviour, Huang et al [42] reported elastic modulus mismatch between the coating and substrate of TiN coatings deposited on AISI M2 HSS substrate, suggesting reduced wear volume in the system. Perhaps this could be the reason why the DCT coated sample performed slightly better with high critical value than the non-DCT coated sample. In addition, comparing the scratch result in terms of the Lc values to the elastic modulus and hardness results, it could be inferred from the result that the main parameters that drives the Lc 1 and Lc 2 values are elastic modulus affecting the coating – substrate, while for the substrate (Lc 3) hardness is considered as the main parameter.

Despite the improvement recorded in Lc values, the average values obtained were low, and was within one standard deviation, hence implying a low level of statistical confidence. Overall, the study shows that DCT works well with PVD-TiN coatings as it causes no damage on the system, however from all indications in the terms of the improvement in the mechanical properties (e.g. hardness, scratch response) it can be inferred that the effect is not significant for PVD-TiN AISI M2 HSS system having been demonstrated in this investigation on the basis of rigorous testing, characterisation and analysis. The present investigation was limited to a thin coating one system. It would also be recommended in the future to investigate the effect of DCT on increased coating thickness as studies show increased coating thickness could have a huge impact on hardness. As well as further investigations are needed on the effect of DCT

on the systems to see if there are any difference in the results. It is also worth looking at in the future for a pre-coating DCT treatment to gauge in details changes to the substrate stiffness, which was suggested as a reason to the coating performance.

4 Conclusions

In this investigation, efforts have been made to investigate the effects of DCT on PVD-TiN coated AISI M2 HSS in order to provide input on the effect and compared with the conventional prepared non-DCT coated samples. Based on this, the following conclusions are reached:

i. On the microstructures, surface morphology of the coating by means of SEM showed that both DCT coated and non-DCT coated samples had a uniform and dense structure typical of PVD-TiN films. Similarly, qualitative analysis of the cross-section by TEM revealed no visible microstructural changes.

ii. Further evaluation, from X-ray diffraction data suggests slight increase in crystallite size and decrease in strain was observed for DCT coated samples but was not significant. Investigation on lattice parameter showed no difference in result, suggesting a minimum level of mismatch at the interface, which could imply that DCT does not cause any damage at the interface.

iii. Mechanical tests such as elastic modulus and hardness results showed improvement for DCT PVD-TiN AISI M2 HSS samples. Confirming that DCT could contribute to improving mechanical properties such as above. The evidence that supports this is that the best results in elastic modulus and hardness were obtained for DCT coated samples compared to non-DCT coated samples. The reason for this was not only attributed to DCT, but also attributed to a combination of the substrate properties.

iv. Examination from the coating scratch response showed that all samples were characterised by a combination of coating failures – chevron, transverse and tensile

cracks, differentiated by their Lc values with standard deviation suggesting no significant difference in values. While the statistics appear to obscure the interpretation, a clear trend was found and in favour of DCT coated sample. A comparison of the Lc values showed that DCT coated samples had Lc values 3.62 (± 3.02) % lower than non-DCT samples. It was also determined that the main parameters that drive the Lc 1 and Lc 2 values were the elastic modulus, while the Lc 3 attributed to hardness.

v. Despite the improvement, the average values obtained were low, and was within one standard deviation, hence implying a low level of statistical confidence. Overall, the study shows that DCT works well with PVD-TiN coatings as it causes no damage on the system, however from all indications in the terms of the improvement in the mechanical properties it can be inferred that the effect is not significant for PVD-TiN AISI M2 HSS system having been demonstrated in this investigation.

Acknowledgements

The authors wish to acknowledge EPSRC IMPaCT CDT (Grant No. EP/R512308/1 & EP/L016206/1) in innovative Metal Processing (IMPaCT), Jim Benson at Cryogenics Ltd (industrial partner), the Advanced Microscopy Facility (AMF) at University of Leicester, and Loughborough Materials Characterisation Centre at Loughborough University and the assistance of Dr Stuart Robertson and Dr Zhaoxia Zhou for help in TEM work.

Declaration of competing interest

The authors declare no conflict of interest

References

[1] P.A. Dearnley, Introduction to Surface Engineering, Cambridge University Press, Cambridge, 2017.
[2] S. Zhang, W. Zhu, TiN coating of tool steels: a review, Journal of Materials Processing Technology 39(1) (1993) 165-177.
[3] J.E. Sundgren, Structure and properties of TiN coatings, Thin Solid Films 128(1) (1985) 21-44.
[4] J.E. Sundgren, B.O. Johansson, S.E. Karlsson, H.T.G. Hentzell, Mechanisms of reactive sputtering of titanium nitride and titanium carbide II: Morphology and structure, Thin Solid Films 105(4) (1983) 367-384.
[5] K.-D. Bouzakis, N. Michailidis, Physical Vapor Deposition (PVD), in: P. The International Academy for, L. Laperrière, G. Reinhart (Eds.), CIRP Encyclopedia of Production Engineering, Springer Berlin Heidelberg, Berlin, Heidelberg, 2014, pp. 1-8.
[6] P. Jovičević-Klug, G. Puš, M. Jovičević-Klug, B. Žužek, B. Podgornik, Influence of heat treatment parameters on effectiveness of deep cryogenic treatment on properties of high-speed steels, Materials Science and Engineering: A 829 (2022).
[7] T. Slatter, R. Thornton, 2.15 Cryogenic Treatment of Engineering Materials, in: M.S.J. Hashmi (Ed.), Comprehensive Materials Finishing, Elsevier, Oxford, 2017, pp. 421-454.
[8] S.S. Gill, J. Singh, R. Singh, H. Singh, Effect of cryogenic treatment on AISI M2 high speed steel: Metallurgical and mechanical characterization, Journal of Materials Engineering and Performance 21(7) (2012) 1320-1326.
[9] D. Mohan Lal, S. Renganarayanan, A. Kalanidhi, Cryogenic treatment to augment wear resistance of tool and die steels, Cryogenics 41(3) (2001) 149-155.
[10] D.G. Fantineli, C.T. Parcianello, T.S. Rosendo, A. Reguly, M.D. Tier, Effect of heat and cryogenic treatment on wear and toughness of HSS AISI M2, Journal of Materials Research and Technology 9(6) (2020) 12354-12363.
[11] C.I. Chiadikobi, Investigating the effects of cryogenic treatments on PVD TiN coated – AISI M2 high speed steel substrate system, School of Engineering, University of Leicester, Leicester, United Kingdom, 2024.
[12] U.M. Chaudry, H.M.R. Tariq, N. Ansari, S.Y. Lee, T.-S. Jun, Room and cryogenic deformation behavior of AZ61 and AZ61-xCaO (x= 0.5, 1 wt.%) alloy, Journal of Magnesium and Alloys (2024).
[13] Y. Noh, M.-S. Lee, U.M. Chaudry, T.-S. Jun, Effect of strain rate on the deformation of 6061-T6 aluminum alloy at cryogenic temperature, Materials Characterization 206 (2023) 113403.
[14] U.M. Chaudry, G. Han, Y. Noh, T.-S. Jun, Effect of Ca alloying and cryogenic temperature on the slip transmission across the grain boundary in pure Mg, Journal of Alloys and Compounds 950 (2023) 169828.
[15] P. Jovicevic-Klug, B. Podgornik, Comparative study of conventional and deep cryogenic treatment of AISI M3:2 (EN 1.3395) high-speed steel, Journal of Materials Research and Technology 9(6) (2020) 13118-13127.
[16] S. Zhirafar, A. Rezaeian, M. Pugh, Effect of cryogenic treatment on the mechanical properties of 4340 steel, Journal of Materials Processing Technology 186(1) (2007) 298-303.
[17] A. Molinari, M. Pellizzari, S. Gialanella, G. Straffelini, K.H. Stiasny, Effect of deep cryogenic treatment on the mechanical properties of tool steels, Journal of Materials Processing Technology 118(1) (2001) 350-355.
[18] D. Yun, Xiaoping L., Hongshen, X., Deep Cryogenic Treatment of High-speed steel and its Mechanism, Heat Treat. Met. 3 (1998) 55-59.
[19] U.M. Chaudry, H.M.R. Tariq, N. Ansari, C.-S. Kim, S.Y. Lee, T.-S. Jun, Exceptional improvement in the yield strength of AZ61 magnesium alloy via cryo-stretching and its implications on the grain growth during annealing, Journal of Alloys and Compounds 970 (2024) 172630.
[20] P. Jovičević-Klug, M. Jenko, M. Jovičević-Klug, B. Šetina Batič, J. Kovač, B. Podgornik, Effect of deep cryogenic treatment on surface chemistry and microstructure of selected high-speed steels, Applied Surface Science 548 (2021).

[21] D. Das, A.K. Dutta, V. Toppo, K.K. Ray, Effect of Deep Cryogenic Treatment on the Carbide Precipitation and Tribological Behavior of D2 Steel, Materials and Manufacturing Processes 22(4) (2007) 474-480.
[22] D.N. Collins, J. Dormer, Deep cryogenic treatment of a D2 cold-work tool steel, Heat Treat. Met. 24(3) (1997) 71-74.
[23] H.M.R. Tariq, U.M. Chaudry, C.-S. Kim, T.-S. Jun, Synergetic improvement in strength and ductility of AZX211 Mg alloy facilitated by {10–12}-{01–12} twin-twin interactions during pre-stretching at cryogenic temperature, Journal of Materials Research and Technology 29 (2024) 3249-3254.
[24] V.D. Mote, Y. Purushotham, B.N. Dole, Williamson-Hall analysis in estimation of lattice strain in nanometer-sized ZnO particles, Journal of Theoretical and Applied Physics 6(1) (2012) 6.
[25] P. Bindu, S. Thomas, Estimation of lattice strain in ZnO nanoparticles: X-ray peak profile analysis, Journal of Theoretical and Applied Physics 8(4) (2014) 123-134.
[26] G.M. Pharr, and Oliver, W.C.,, Measurement of Thin Film Mechanical Properties Using Nanoindentation, MRS Bulletin 17(7) (1992) 28-33.
[27] W.C. Oliver, G.M. Pharr, An improved technique for determining hardness and elastic modulus using load and displacement sensing indentation experiments, Journal of Materials Research 7(6) (1992) 1564-1583.
[28] W.C. Oliver, G.M. Pharr, Measurement of hardness and elastic modulus by instrumented indentation: Advances in understanding and refinements to methodology, Journal of Materials Research 19(1) (2004) 3-20.
[29] G. Krauss, 22-Surface Modification. Steels: Processing, Structure, and Performance, ASM International (2015) 552-577.
[30] T. Vieira, Castanho, J., Louro, C.,, 16-Hard Coatings Based on Metal Nitrides, Metal Carbides and Nanocomposite Materials: PVD Process and Properties, Materials Surface Processing by Directed Energy Techniques (2006) 537-572.
[31] M. Walczak, Pasierbiewicz, K., Szala, M., Adhesion and Mechanical Properties of TiAlN and AlTiN Magnetron Sputtered Coatings Deposited on the DMSL Titanium Alloy Substrate, Acta Physica Polonica A 136 (2019) 294-298.
[32] F. Attar, T. Johannesson, Adhesion evaluation of thin ceramic coatings on tool steel using the scratch testing technique, Surface and Coatings Technology 78(1) (1996) 87-102.
[33] I. Standard, Fine Ceramics (advanced ceramics, advanced technical) – Determination of adhesion of ceramic coatings by scratch testing, ISO 20502:2005(E) (2005).
[34] T. Bhushan, A. Chandrashekhar, S. Venkat Prasat, I. Rajasri Reddy, Effect Of Substrate Surface Roughness On Adhesion Of Titanium Nitride Coatings Deposited By Physical Vapour Deposition Technique, IOP Conference Series: Materials Science and Engineering 981(4) (2020) 042022.
[35] P. Saikia, A. Joseph, R. Rane, B.K. Saikia, S. Mukherjee, Role of substrate and deposition conditions on the texture evolution of titanium nitride thin film on bare and plasma-nitrided high-speed steel, Journal of Theoretical and Applied Physics 7(1) (2013) 66.
[36] A.K. Krella, Chapter 16 - Degradation of protective PVD coatings, in: A.S.H. Makhlouf, M. Aliofkhazraei (Eds.), Handbook of Materials Failure Analysis with Case Studies from the Chemicals, Concrete and Power Industries, Butterworth-Heinemann2016, pp. 411-440.
[37] J. Haider, M. Rahman, B. Corcoran, M.S.J. Hashmi, Simulation of thermal stress in magnetron sputtered thin coating by finite element analysis, Journal of Materials Processing Technology 168(1) (2005) 36-41.
[38] G. Kimmel, L. Politi, T. Wieder, Characterization of TiN Film by XRD and XRF, Advances in X-Ray Analysis 37 (1993) 175-182.
[39] K. Ponhan, K. Tassenberg, D. Weston, K.G.M. Nicholls, R. Thornton, Effect of SiC nanoparticle content and milling time on the microstructural characteristics and properties of Mg-SiC nanocomposites synthesized with powder metallurgy incorporating high-energy ball milling, Ceramics International 46(17) (2020) 26956-26969.

[40] S.J. Bull, Failure modes in scratch adhesion testing, Surface and Coatings Technology 50(1) (1991) 25-32.
[41] P. Hedenqvist, M. Olsson, S. Jacobson, S. Söderberg, Failure mode analysis of TiN-coated high speed steel: In situ scratch adhesion testing in the scanning electron microscope, Surface and Coatings Technology 41(1) (1990) 31-49.
[42] X. Huang, I. Etsion, T. Shao, Effects of elastic modulus mismatch between coating and substrate on the friction and wear properties of TiN and TiAlN coating systems, Wear 338-339 (2015) 54-61.

Tables

Table I. Chemical composition of AISI M2 HSS

Wt%	Mo	Cr	V	W	P	Mn	S	Si	C	Fe
AISI M2	4.86	4.2	1.89	6.05	0.33	0.33	0.01	0.31	0.89	Bal

Table II: Average surface roughness

Surface Roughness	**Ra Value**
Theoretical value	(0.02 – 0.09) ± 0.05 µm
Experimental value: Q+T+Coat	0.0514 ± 0.001 µm
Experimental value: Q+T+Coat+DCT	0.0519 ± 0.001 µm
Experimental value: Q+T	0.04 ± 0.002 µm

Table III: SEM-EDS elemental composition and coating thickness

Samples	**Elemental composition (wt%)**	**Coating thickness**
Q+T+Coat	Ti: 77.24; N: 22.76	2.33 ± (0.05) µm
Q+T+Coat+DCT	Ti: 78.26; N: 21.74	2.33 ± (0.03) µm

Table IV: Interplanar spacing and lattice parameters of TiN planes

Crystalline Planes	**2θ (°)**	**Q+T+Coat: d (nm)**	**Q+T+Coat+DCT: d (nm)**	**Q+T+Coat: a (nm)**	**Q+T+Coat+DCT: a (nm)**
(111)	36.51°	0.243± 0.05	0.245±0.05	0.428±0.001	0.425±0.001

(200)	42.57°	0.212±0.05	0.213±0.05	0.425±0.001	0.425±0.001
(220)	61.37°	0.151±0.05	0.151±0.05	0.428±0.001	0.427±0.001
(311)	72.26°	0.129±0.05	0.128± 0.05	0.427±0.001	0.425±0.001
(222)	77.61°	0.123±0.05	0.123±0.05	0.426±0.001	0.426±0.001

Table V: Interplanar spacing and lattice parameters of the substrate (α-Fe) planes

Crystalline Planes	**2θ (°)**	**Q+T+Coat: d (nm)**	**Q+T+Coat+DCT: d (nm)**	**Q+T+Coat: a (nm)**	**Q+T+Coat+DCT: a (nm)**
(110)	44.25°	0.205±0.04	0.205±0.04	0.290±0.001	0.290±0.001
(200)	64.37°	0.145±0.04	0.145±0.04	0.289±0.001	0.290±0.001
(211)	81.62°	0.118±0.04	0.118±0.04	0.289±0.001	0.290±0.001

Table VI: Hardness and modulus of the samples

Material condition (Coating/substrate)	**Elastic Modulus (GPa)**	**Indentation Hardness (GPa)**	**Elastic Modulus ratio (GPa) Eco/Esu**
Q+T+Coat	267.46 ± 13.40	20.15 ± 1.46	--
Q+T+Coat+DCT	307.07 ± 14.05	21.19 ± 1.34	--
Q+T	169.41 ± 17.56	7.14 ± 1.21	--
Q+T+DCT	184.54 ± 13.06	7.86 ± 0.80	--
Q+T+Coat – Eco/Esu	--	--	1.58 ± 0.04
Q+T+Coat+DCT - Eco/Esu	--	--	1.66 ± 0.04

Table VII: T - statistics

T-statistics (Q+T+Coat & Q+T+Coat+DCT) Modulus	**T-statistics (Q+T & Q+T+DCT) Modulus**	**T-statistics (Q+T+Coat & Q+T+Coat+DCT) Hardness**	**T-statistics (Q+T & Q+T+DCT) Hardness**

(P-value)	**(P-value)**	**(P-value)**	**(P-value)**
2.2572E-19 (Significant)	4.67168E-05 (Significant)	0.001248 (Significant)	0.002026 (Significant)

Table VIII: Summary of Lc values and standard deviation

Samples	Lc 1 (N)	Lc 2 (N)	Lc 3 (N)
Q+T+Coat	16.44 ± 2.08	47.47 ± 2.03	55.82 ± 2.92
Q+T+Coat+DCT	19.47 ± 1.70	49.32 ± 2.02	57.84 ± 3.11

List of Figure captions

Figure 1: SEM surface morphology of the TiN coating (a) Q+T+Coat (b) Q+T+Coat+DCT

Figure 2: Coating particle size distribution (a) Q+T+Coat (b) Q+T+Coat+DCT

Figure 3: EDS line scan (a) Q+T+Coat (b) Q+T+Coat+DCT

Figure 4: SEM micrograph of the coating cross-section (a) Q+T+Coat (b) Q+T+Coat+DCT

Figure 5: TEM micrograph of the coating cross – section (a) Q+T+Coat (b) Q+T+Coat+DCT

Figure 6: XRD patterns of the samples

Figure 7: Plot of $\beta t \cos \theta$ against $4 \sin \theta$ for Q+T+Coat

Figure 8: Plot of $\beta t \cos \theta$ against $4 \sin \theta$ for Q+T+Coat+DCT

Figure 9: SEM micrograph of indentation impression made in (a) Q+T+Coat (b) Q+T+Coat+DCT sample

Figure 10: SEM micrograph showing cracks around the edges of the imprint (a) Q+T+Coat (b) Q+T+Coat+DCT sample

Figure 11: (a) Split-up image from optical microscope showing the scratch tracks from complete to the substrate exposure for Q+T+Coat sample. SEM micrograph showing the Lc positions and cracks observed: (b) Lc 1 – 16.44 N (c) Lc 2 – 47.47 N (d) Lc 3 – 55.82 N

Figure 12: (e) Split-up image from optical microscope showing the scratch tracks from complete to the substrate exposure for Q+T+Coat+DCT sample. SEM micrograph showing the Lc positions and cracks observed: (f) Lc 1 – 19.47 N (g) Lc 2 – 49.32 N (h) Lc 3 – 57.84 N

Figures

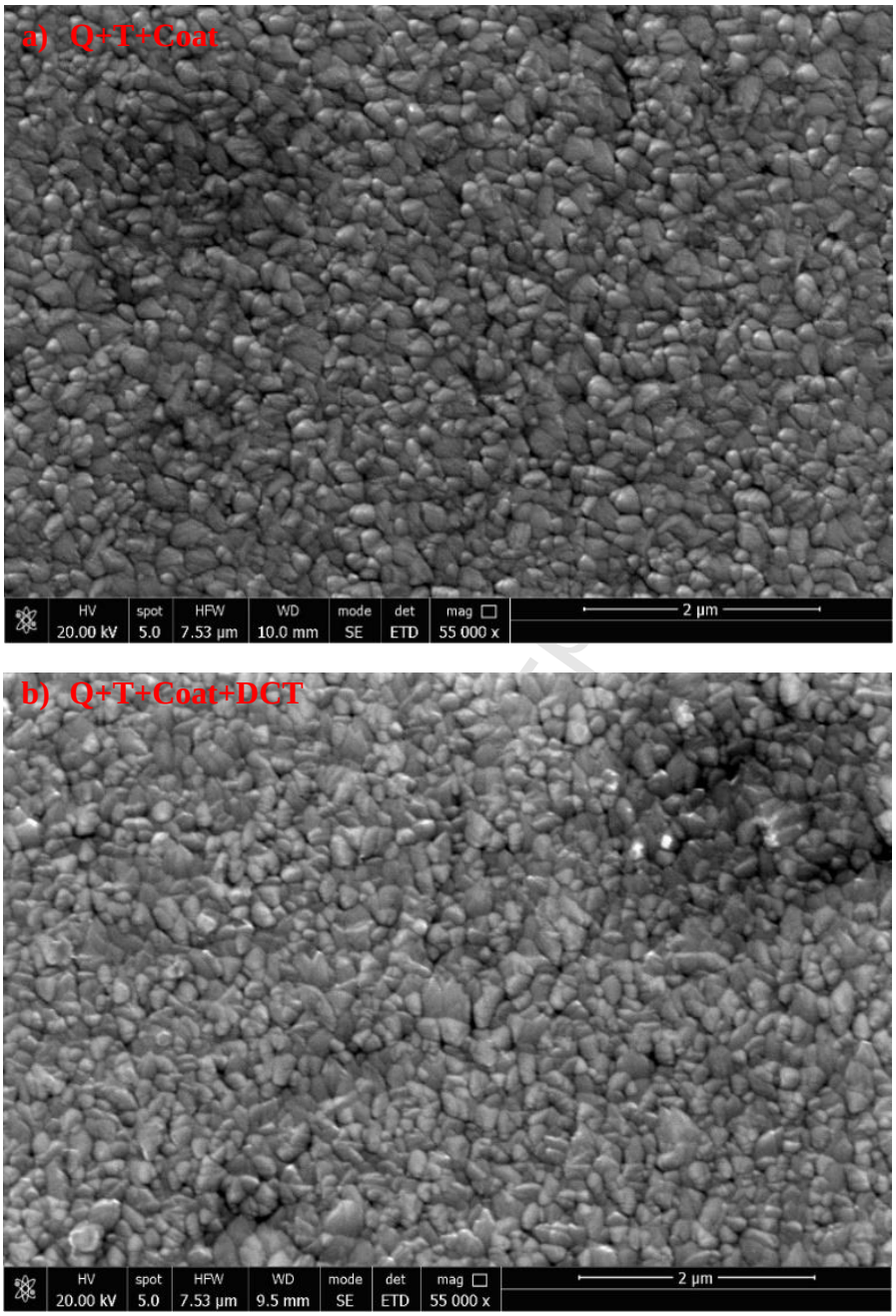

Figure 1: (a) Q+T+Coat (b) Q+T+Coat+DCT

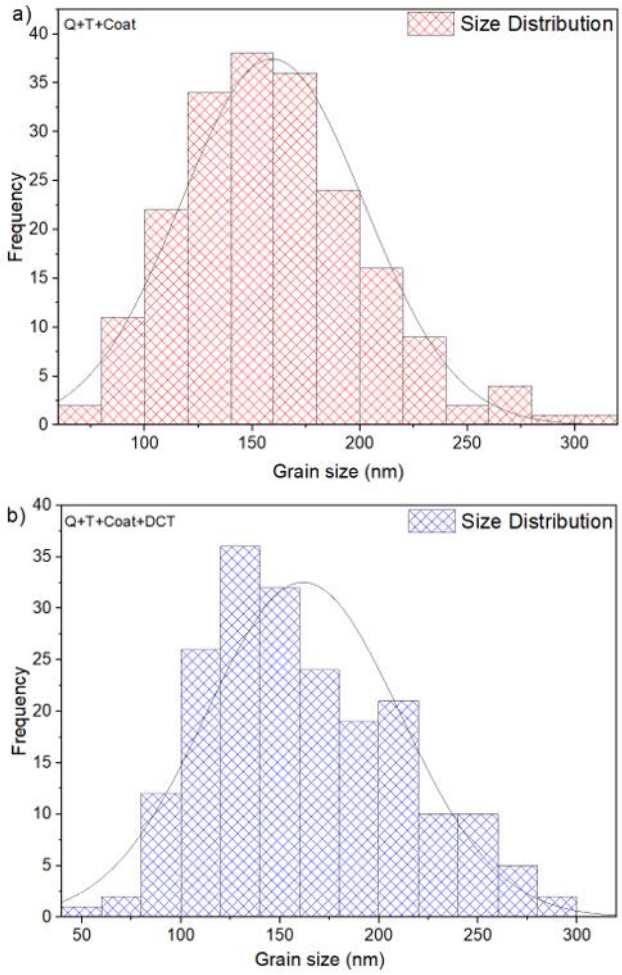

Figure 2: (a) Q+T+Coat (b) Q+T+Coat+DCT

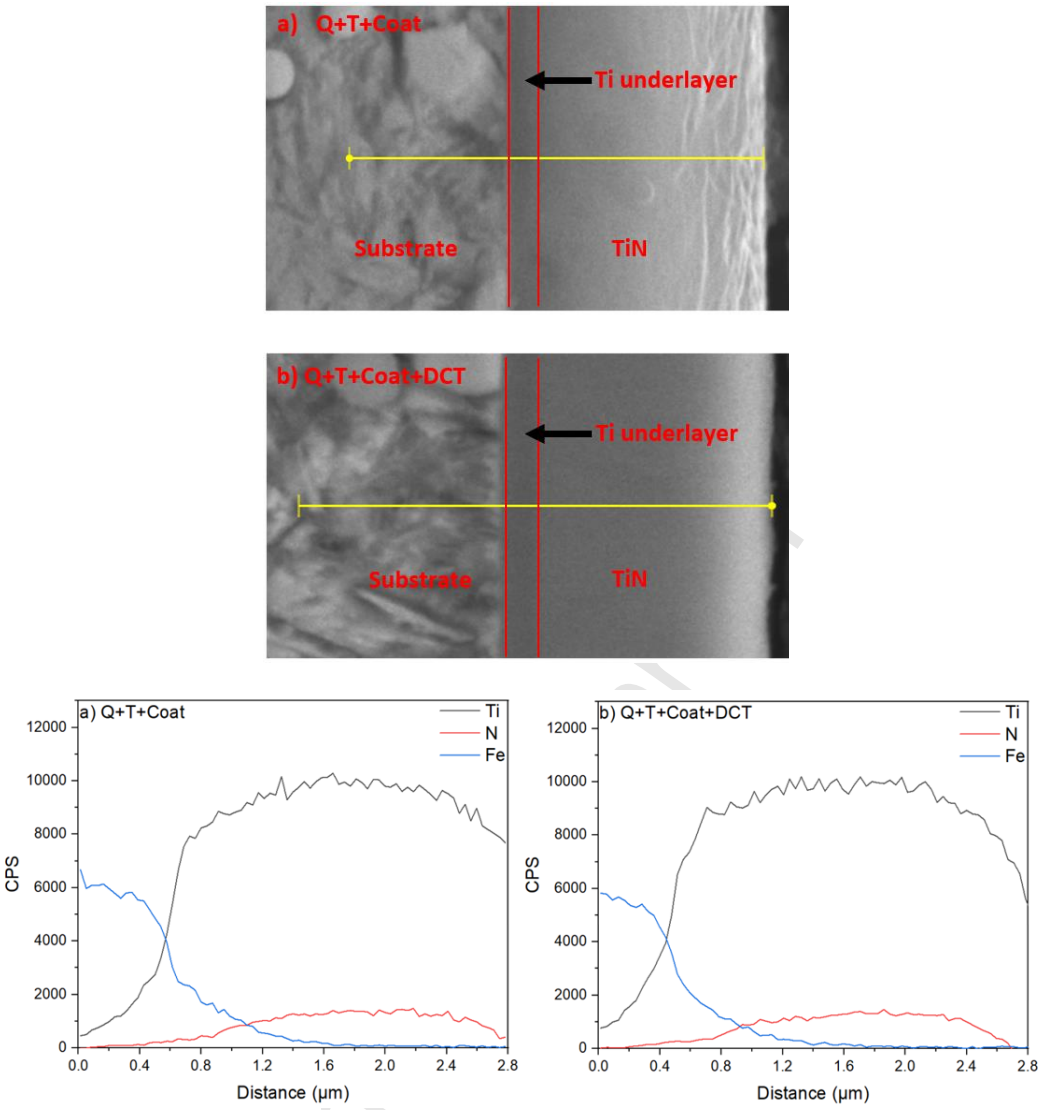

Figure 3: (a) Q+T+Coat (b) Q+T+Coat+DCT

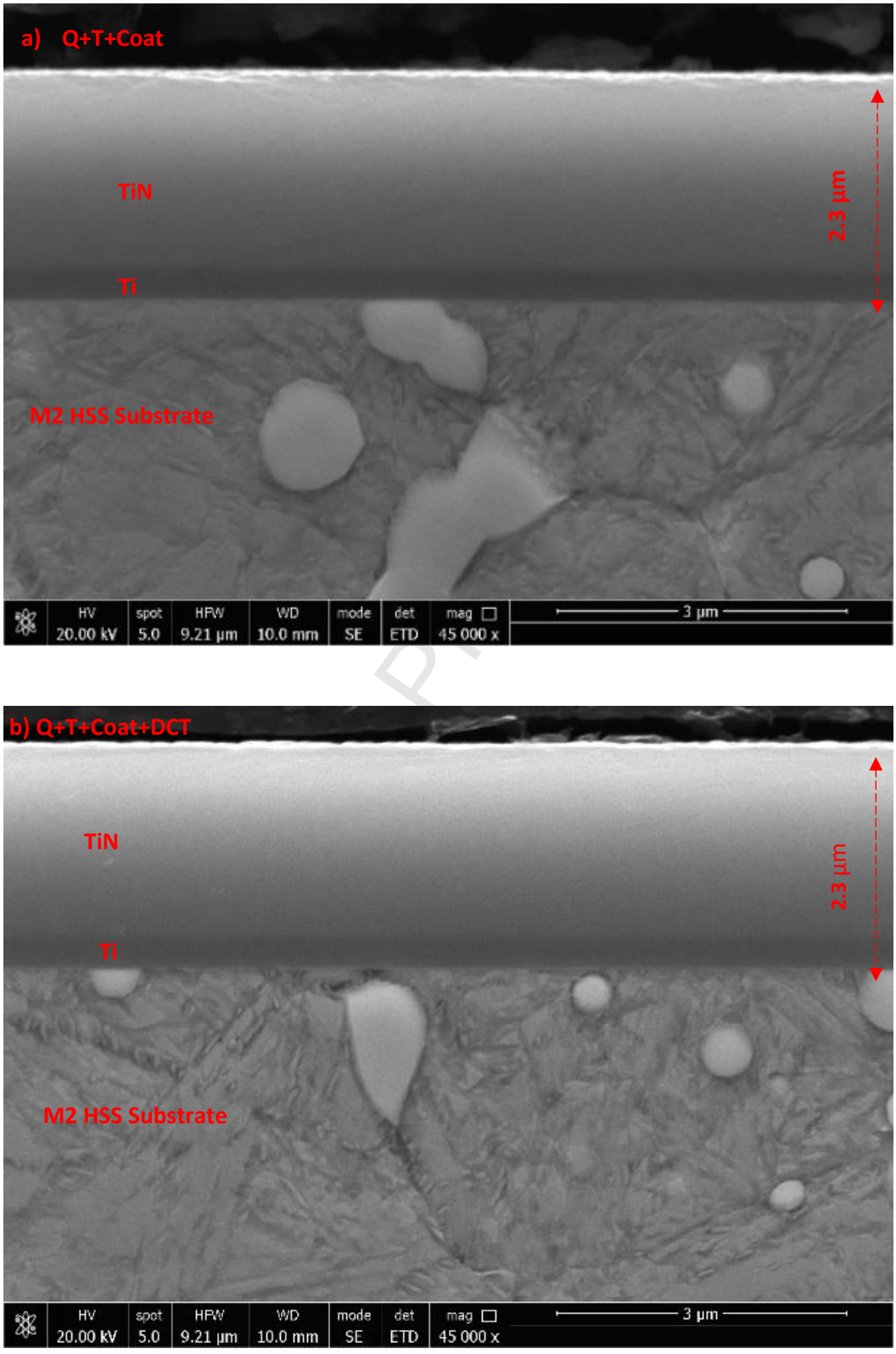

Figure 4: (a) Q+T+Coat (b) Q+T+Coat+DCT

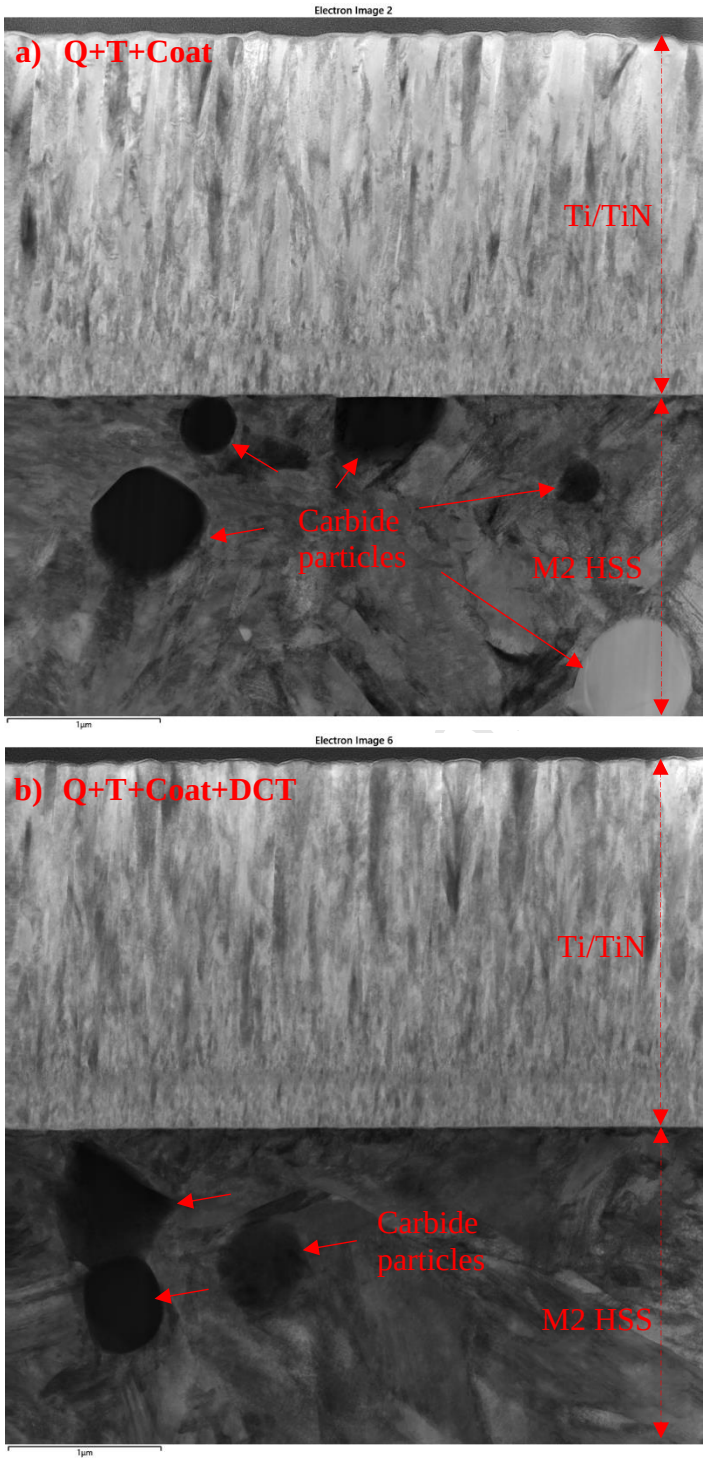

Figure 5: (a) Q+T+Coat (b) Q+T+Coat+DCT

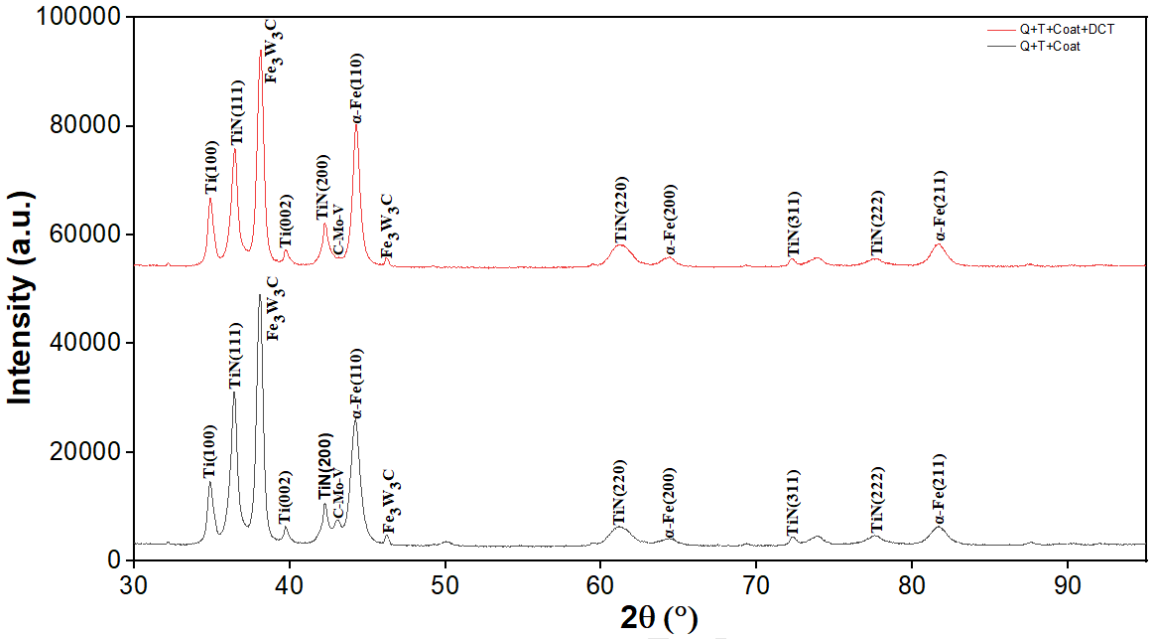

Figure 6

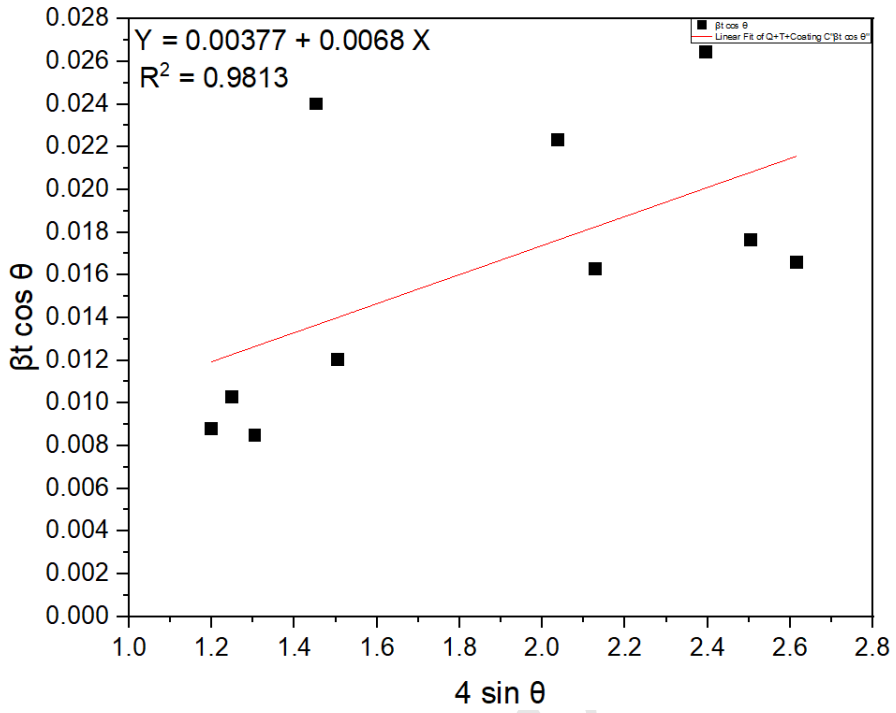

Figure 7

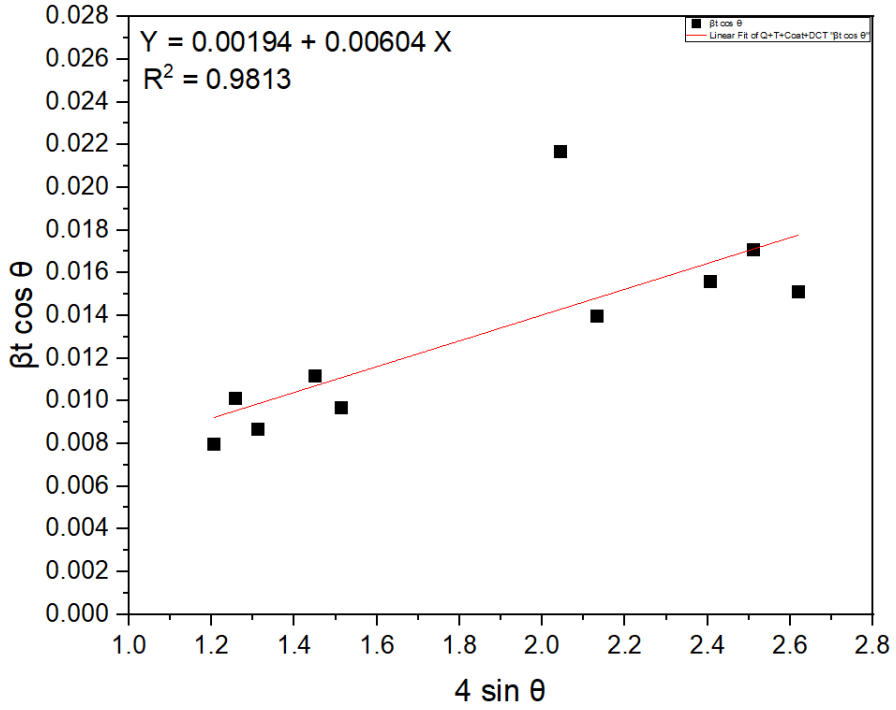

Figure 8

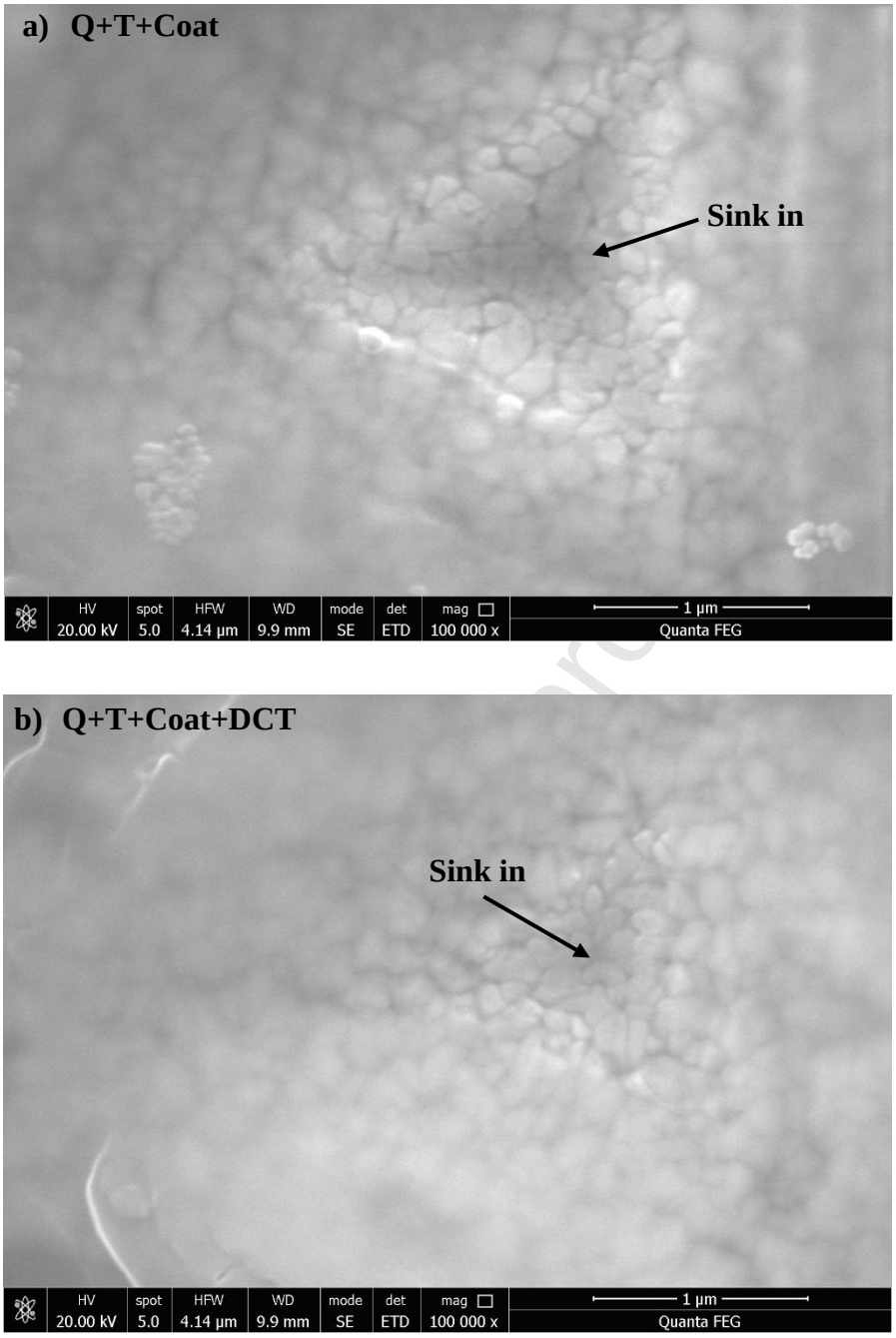
a) Q+T+Coat
Sink in
HV
20.00 kV
spot
5.0
HFW
4.14 µm
WD
9.9 mm
mode
SE
det
ETD
mag
100 000 x
1 µm
Quanta FEG
b) Q+T+Coat+DCT
Sink in
HV
20.00 kV
spot
5.0
HFW
4.14 µm
WD
9.9 mm
mode
SE
det
ETD
mag
100 000 x
1 µm
Quanta FEG

Figure 9

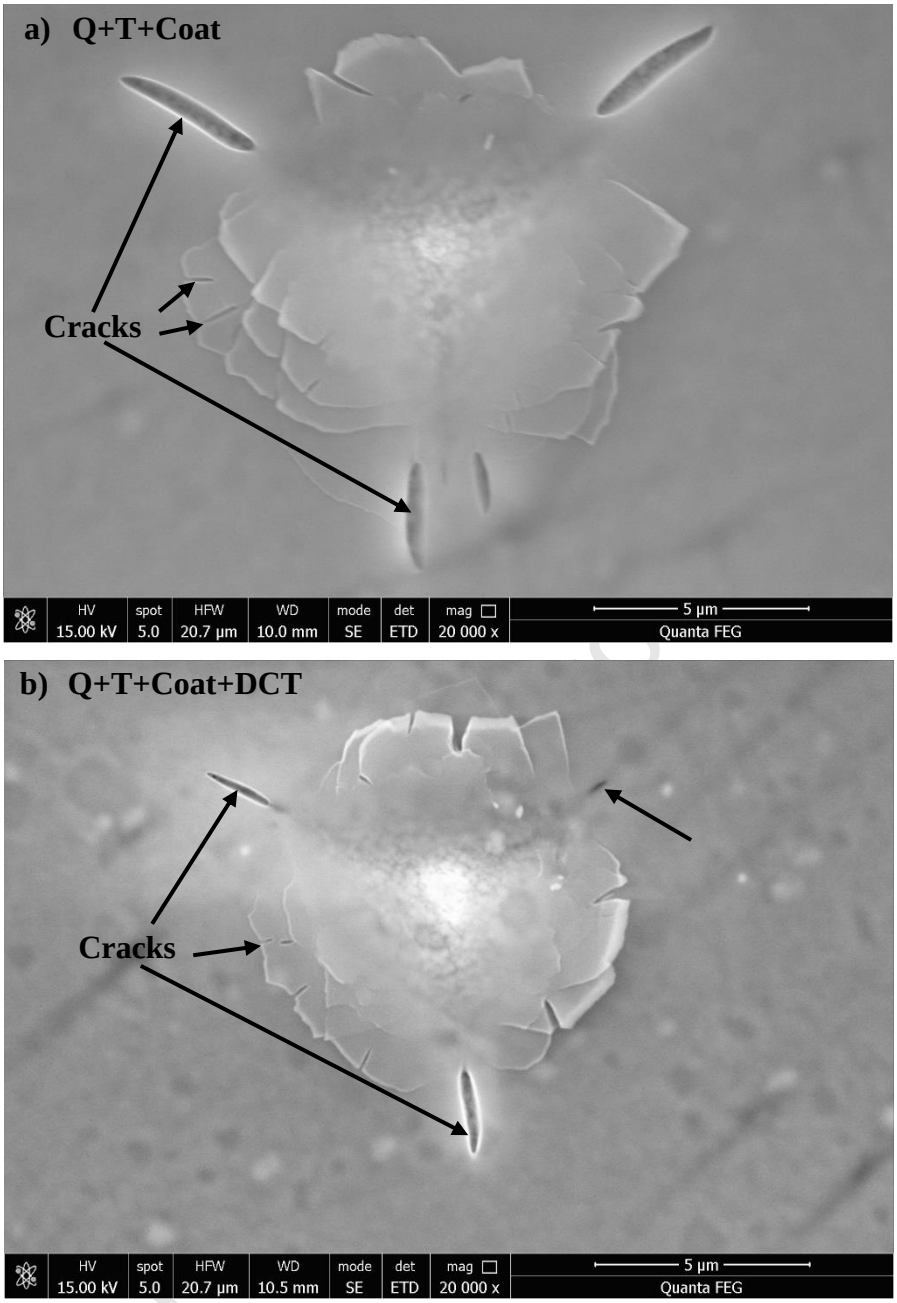
a) Q+T+Coat
Cracks
HV 15.00 kV
spot 5.0
HFW 20.7 µm
WD 10.0 mm
mode SE
det ETD
mag 20 000 x
5 µm
Quanta FEG
b) Q+T+Coat+DCT
Cracks
HV 15.00 kV
spot 5.0
HFW 20.7 µm
WD 10.5 mm
mode SE
det ETD
mag 20 000 x
5 µm
Quanta FEG

Figure 10

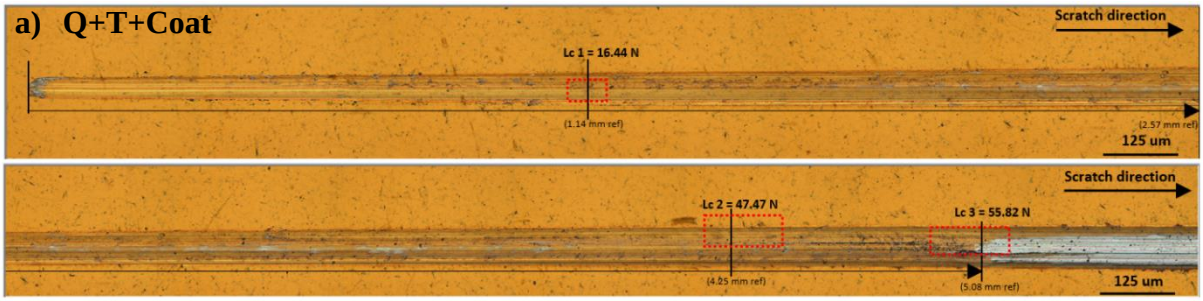
a) Q+T+Coat
Scratch direction
Lc 1 = 16.44 N
(1.14 mm ref)
(2.57 mm ref)
125 um
Scratch direction
Lc 2 = 47.47 N
Lc 3 = 55.82 N
(4.25 mm ref)
(5.08 mm ref)
125 um

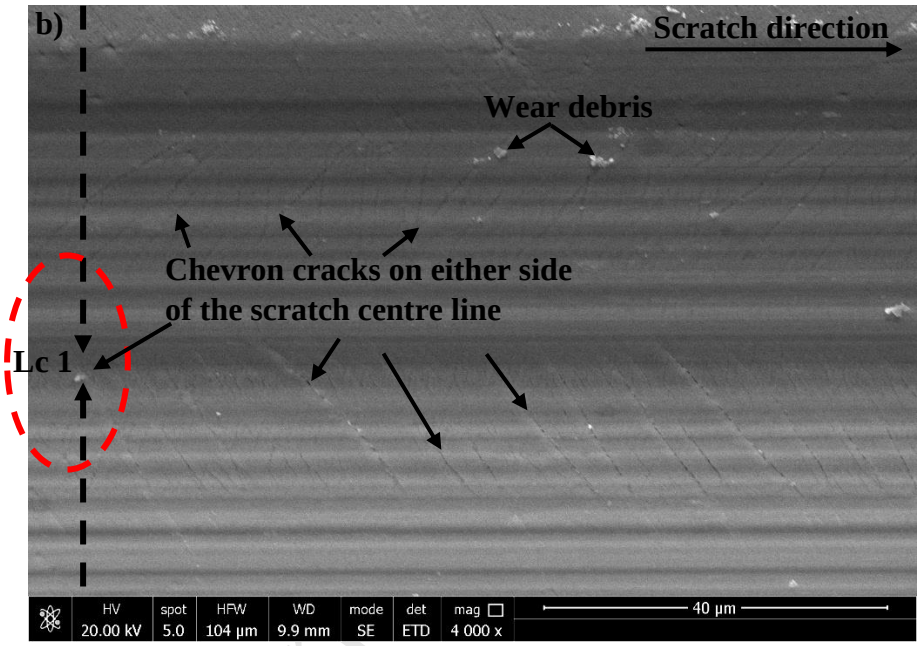
b)
Scratch direction
Wear debris
Chevron cracks on either side
of the scratch centre line
Lc 1
HV
20.00 kV
spot
5.0
HFW
104 µm
WD
9.9 mm
mode
SE
det
ETD
mag
4 000 x
40 µm

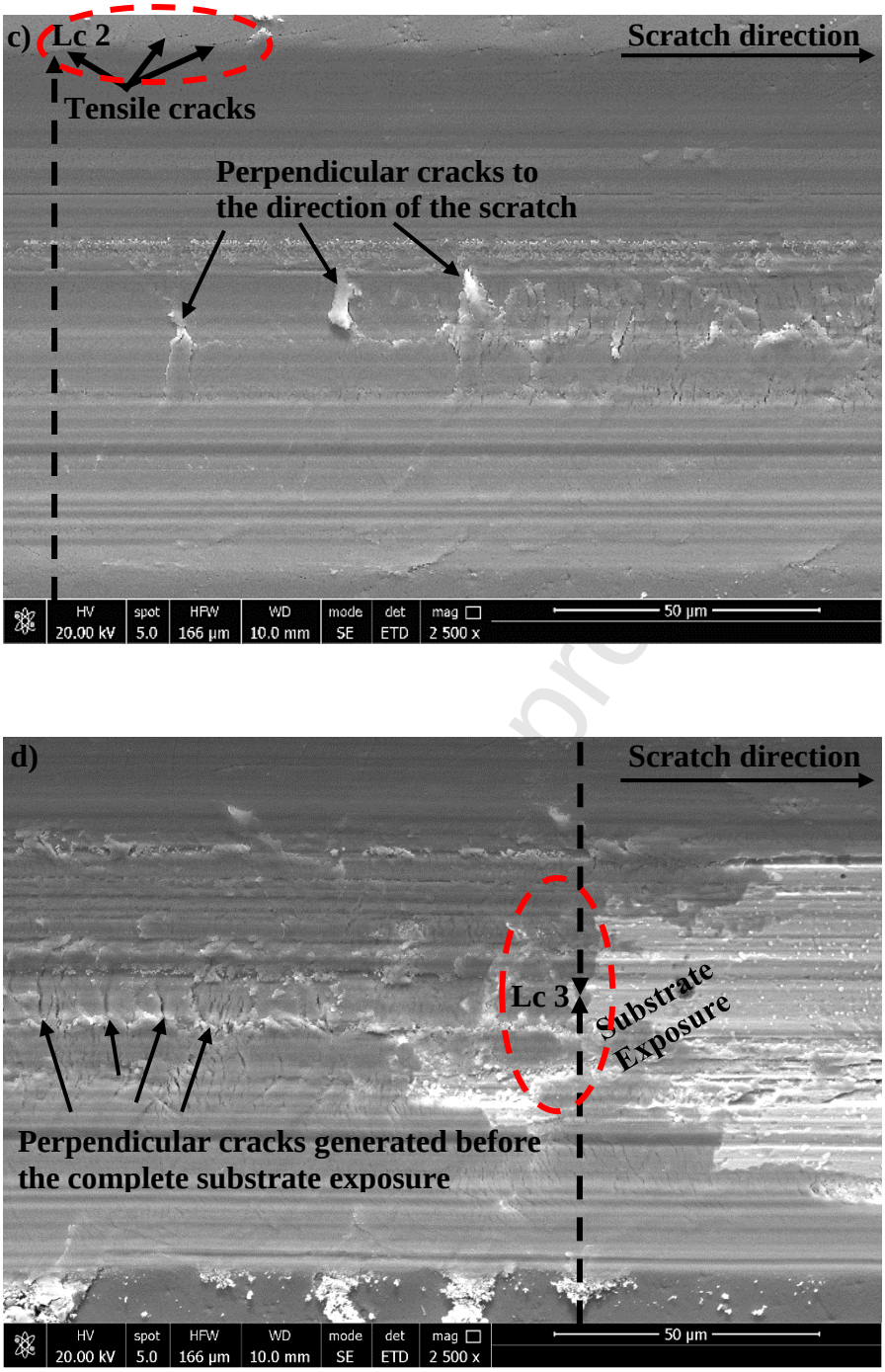
c)
Lc 2
Tensile cracks
Scratch direction
Perpendicular cracks to
the direction of the scratch
HV 20.00 kV
spot 5.0
HFW 166 µm
WD 10.0 mm
mode SE
det ETD
mag 2 500 x
50 µm
d)
Scratch direction
Lc 3
Substrate
Exposure
Perpendicular cracks generated before
the complete substrate exposure
HV 20.00 kV
spot 5.0
HFW 166 µm
WD 10.0 mm
mode SE
det ETD
mag 2 500 x
50 µm

Figure 11

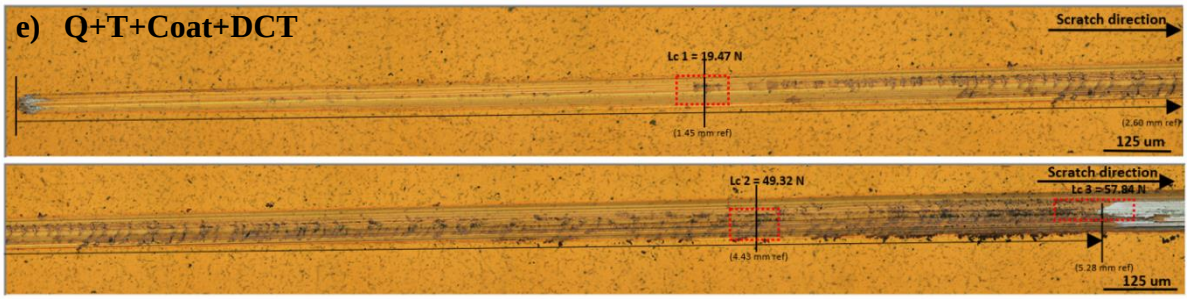
e) Q+T+Coat+DCT
Scratch direction
Lc 1 = 19.47 N
125 um
Lc 2 = 49.32 N
Scratch direction
125 um

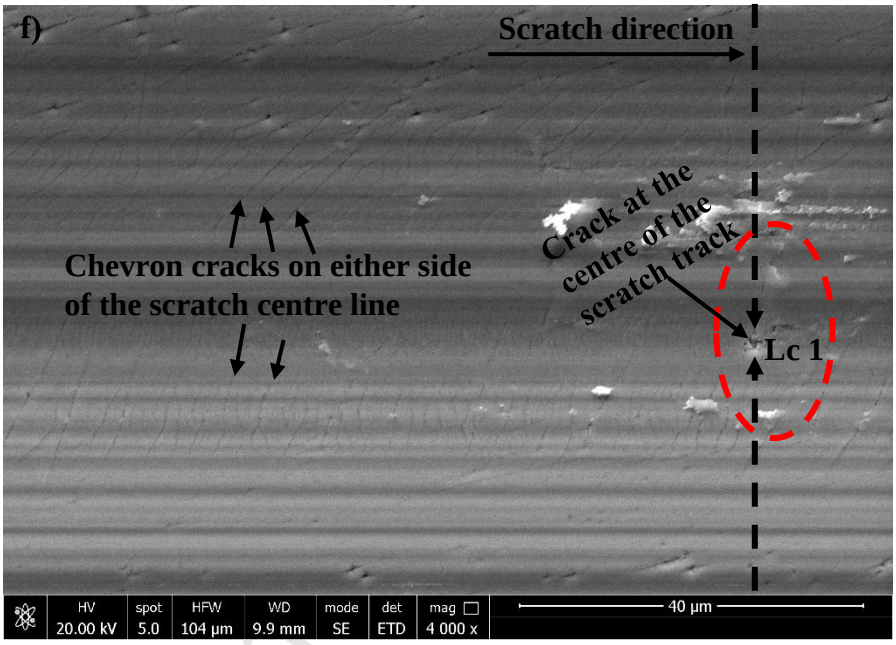
f)
Scratch direction
Chevron cracks on either side of the scratch centre line
Crack at the centre of the scratch track
Lc 1
HV 20.00 kV
spot 5.0
HFW 104 µm
WD 9.9 mm
mode SE
det ETD
mag 4 000 x
40 µm

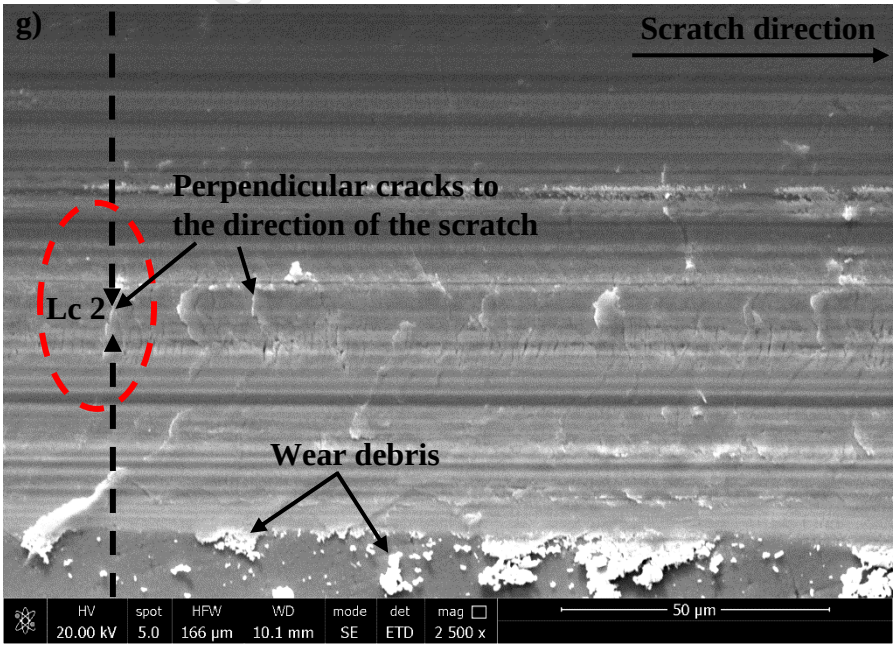
g)
Scratch direction
Perpendicular cracks to the direction of the scratch
Lc 2
Wear debris
HV 20.00 kV
spot 5.0
HFW 166 µm
WD 10.1 mm
mode SE
det ETD
mag 2 500 x
50 µm

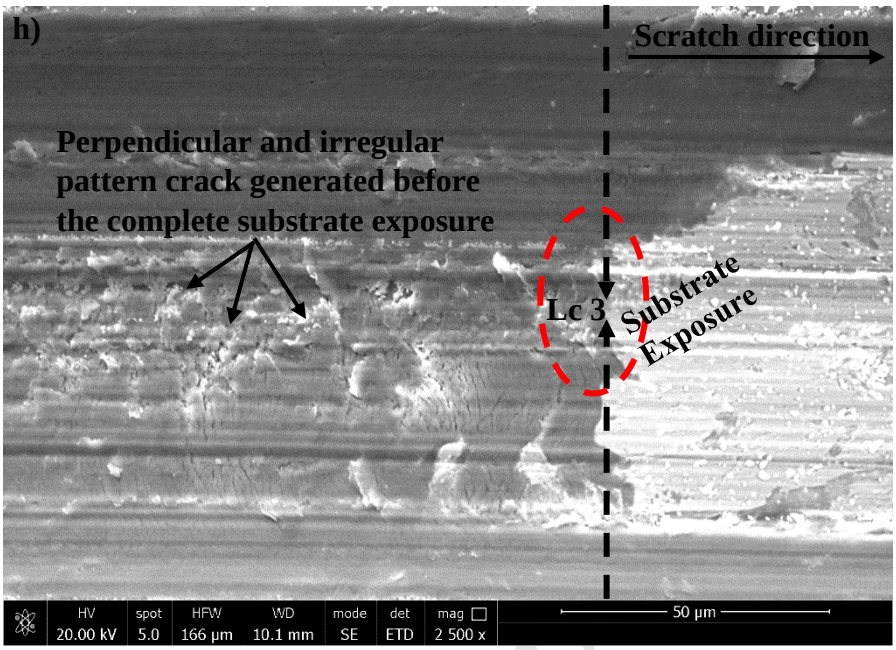

Figure 12

Appendix A

Supplementary data of the as received AISI M2 HSS

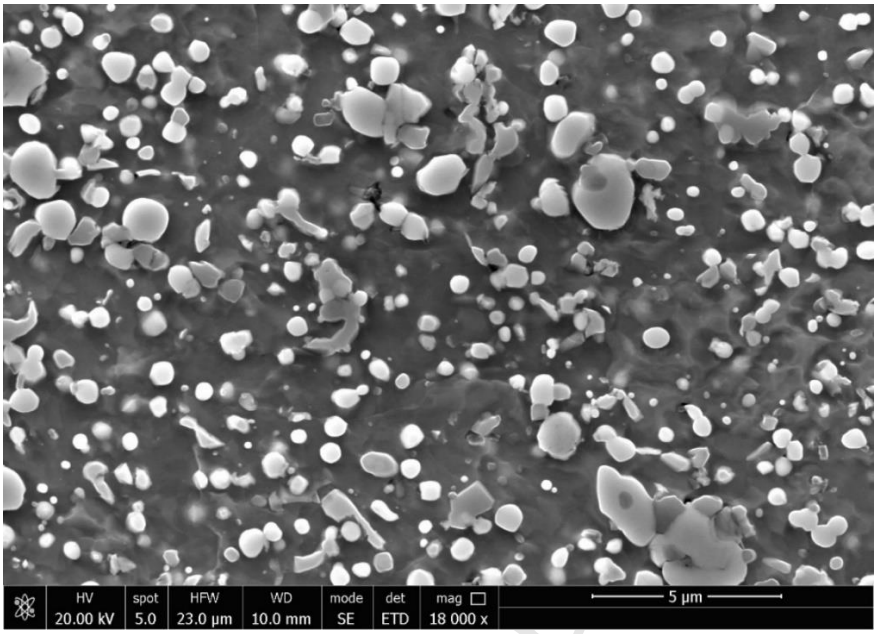

Figure A1: SEM micrograph for the as received AISI M2 HSS

The as received sample (Figure A1) consisting mainly of ferrite and randomly distributed carbides, was heat treated into a hardened and tempered martensite microstructure (Q+T) - Figure A2 below, characterised by largely dominated small carbide particles on the matrix. This microstructure was then coated resulting the result presented in section 3.1 of the result section.

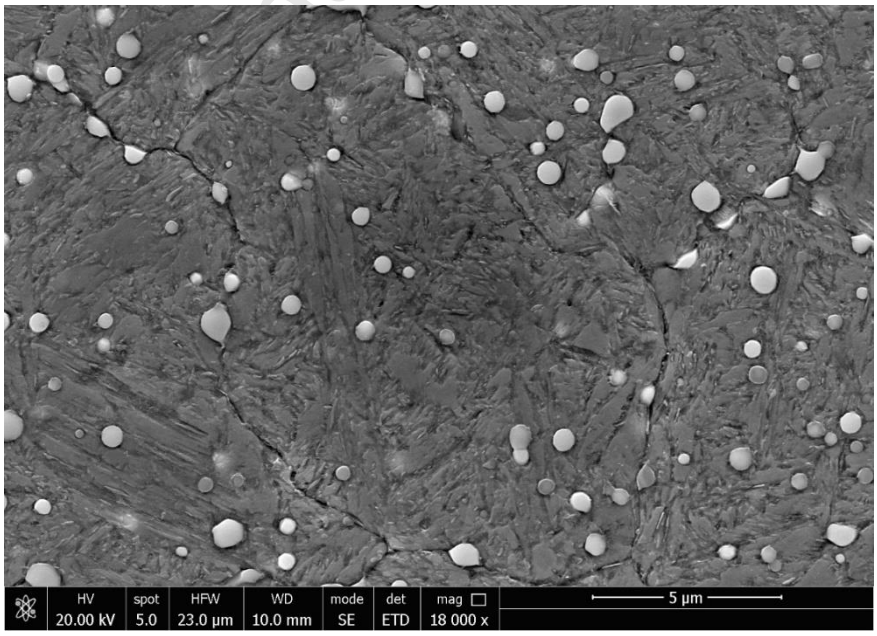

Figure A2: SEM micrograph of the AISI M2 HSS of a

tempered martensite structure

Highlights

- *This paper provides experimental data on the effects of PVD-TiN coated AISI M2 High speed steel subjected to DCT.*
- *Dense transverse cracks are observed for DCT coated samples.*
- *The mechanical properties such as hardness (5.16%) and elastic modulus (14.81%) are improved due to the substrate and changes in the substrate due to DCT.*